12

Nonlinear Elasticity, Plasticity, and Viscoelasticity

The soft-minded man always fears change. He feels security in the status quo, and he has an almost morbid fear of the new. For him, the greatest pain is the pain of a new idea.

——— Dr. Martin Luther King, Jr.

12.1 Introduction

Recall that nonlinearities arise from two independent sources. (1) Nonlinearity due to changes in the geometry or position of the material particles of a continuum, which is called the *geometric nonlinearity.* (2) Nonlinearity due to the nonlinear material behavior, which is called *material nonlinearity.* In solid mechanics, the geometric nonlinearity arises from large strains and/or large rotations, and these enter the formulation through the strain–displacement relations as well as the equations of motion. In fluid mechanics and coupled fluid flow and heat transfer, the geometric nonlinearity arises as a result of the spatial (or Eulerian) description of motion and they enter the equations of motion through material time derivative term. Material nonlinearity in all disciplines of engineering arise from nonlinear relationship between the kinetic and kinematic variables, for example, stress–strain relations, heat flux–temperature gradient relations, and so on. In general, material nonlinearities arise due to the material parameters (e.g. moduli, viscosity, conductivity, etc.) being functions of strains (or their rates), temperature, and other basic variables.

The finite element formulations presented in the previous chapters were largely based on geometric nonlinearity. However, the nonlinearity in the one- and two-dimensional field problems discussed in Chapters 4 and 6 could have come from either sources. In this chapter, material nonlinear formulations are given attention. This field is very broad and special books are devoted to various types of nonlinearities (e.g. plasticity, viscoelasticity, and non-Newtonian materials). The objective of this chapter is to briefly discuss nonlinear elastic and elastic–plastic material models for solids, finite element models of viscoelastic beams with the von Kármán nonlinearity, and the power-law model for viscous incompressible fluids.

J.N. Reddy, *An Introduction to Nonlinear Finite Element Analysis*, Second Edition. Published in 2015 by Oxford University Press.

12.2 Nonlinear Elastic Problems

Materials for which the constitutive behavior is only a function of the current state of deformation are known as *elastic.* In the special case in which the work done by the stresses during a deformation is dependent only on the initial state and the current configuration, the material is called *hyperelastic,* that is, there exists a strain energy density potential $U_0(E_{ij})$ such that

$$S_{ij} = \frac{\partial U_0}{\partial E_{ij}} \tag{12.2.1}$$

where S_{ij} ard E_{ij} are the components of the second Piola–Kirchhoff stress tensor and Green–Lagrange strain tensor, respectively. When U_0 is a nonlinear function of the strains, the body is said to be nonlinearly elastic. A nonlinearly elastic material has the following features: (a) U_0 is a nonlinear function of strains, (b) all of the deformation is recoverable on removal of loads causing the deformation, and (c) there is no loss of energy (i.e. loading and unloading is along the same stress–strain path; see Fig. 12.2.1).

Here we consider a one-dimensional problem to discuss the finite element formulation of a nonlinear elastic material for the case of kinematically infinitesimal strains, for which we have $\sigma_{xx} = S_{xx}$ and $\varepsilon_{xx} = E_{xx}$. Consider the nonlinear uniaxial stress–strain relation

$$\sigma_{xx} = E\ \mathcal{F}(\varepsilon_{xx}) \tag{12.2.2}$$

where ε_{xx} is the infinitesimal strain, E is a material constant, and $\mathcal{F}$ is a nonlinear function of the strain.

The virtual work expression for the axial deformation of a bar made of a nonlinear elastic material is

$$\begin{aligned} 0 &= \int_A \int_{x_a}^{x_b} \sigma_{xx} \delta\varepsilon_{xx}\ dxdA - \int_{x_a}^{x_b} f\delta u\ dx - P_1^e \delta u(x_a) - P_2^e \delta u(x_b) \\ &= \int_{x_a}^{x_b} \left[EA\ \mathcal{F}(\varepsilon_{xx})\delta\varepsilon_{xx} - f\delta u\right] dx - P_1^e \delta u(x_a) - P_2^e \delta u(x_b) \end{aligned} \tag{12.2.3}$$

where P_i^e are the nodal forces. The residual vector for the finite element model is

$$R_i^e = \int_{x_a}^{x_b} \left[EA\ \mathcal{F}(\varepsilon_{xx}) \frac{d\psi_i^e}{dx} - f\psi_i^e \right] dx - P_i^e \tag{12.2.4}$$

where ψ_i^e are the Lagrange interpolation functions. The tangent stiffness matrix coefficients are computed using the relation

$$T_{ij}^e = \frac{\partial R_i^e}{\partial u_j^e} = EA \int_{x_a}^{x_b} \frac{\partial \mathcal{F}}{\partial \varepsilon_{xx}} \frac{\partial \varepsilon_{xx}}{\partial u_j^e} \frac{d\psi_i^e}{dx}\ dx = EA \int_{x_a}^{x_b} \left(\frac{\partial \mathcal{F}}{\partial \varepsilon_{xx}} \right) \frac{d\psi_i^e}{dx} \frac{d\psi_j^e}{dx}\ dx \tag{12.2.5}$$

where small strain assumption is used in arriving at the last step.

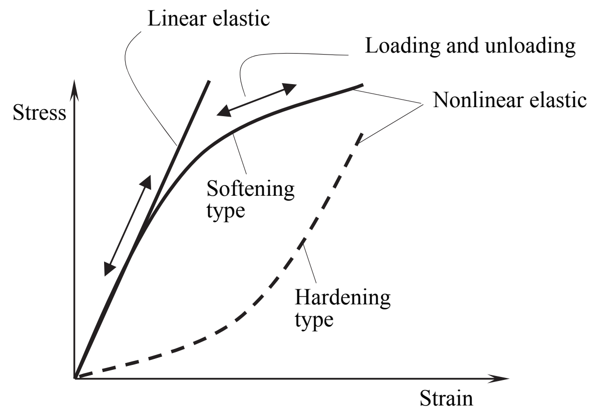

Fig. 12.2.1: A nonlinear elastic stress–strain curve.

An example of the nonlinear elastic response is provided by the Romberg–Osgood model

$$\mathcal{F}(\varepsilon_{xx}) = (\varepsilon_{xx})^n\,, \quad \frac{\partial \mathcal{F}}{\partial \varepsilon_{xx}} = n\,(\varepsilon_{xx})^{n-1} \tag{12.2.6}$$

where $n > 0$ is a material parameter. The value of $n = 1$ yields the linear elastic case. This discussion can be extended to beams, plates, and multi-dimensional cases, where $\mathcal{F} = \mathcal{F}(\varepsilon_{ij})$.

12.3 Small Deformation Theory of Plasticity

12.3.1 Introduction

Plasticity refers to non-recoverable deformation and non-unique stress paths in contrast to nonlinear elasticity, where the entire load–deflection path is unique and the strains are recovered on load removal. The mathematical theory of plasticity is of a phenomenological nature on the macroscopic scale and the objective of the theory is to provide a theoretical description of the relationship between stress and strain for a material that exhibits an elastic–plastic response (see [285–290]; in particular, see pp. 26–29 for one-dimensional bar problems, pp. 129–148 for one-dimensional Timoshenko beams, and pp. 215–281 for two-dimensional problems in [289]). The plastic behavior is characterized by irreversibility of stress paths and the development of permanent (i.e. non-recoverable) deformation (or strain), known as *yielding* (or plastic flow).

If uniaxial behavior of a material is considered, a nonlinear stress–strain relationship on loading alone does not determine if nonlinear elastic or plastic behavior is exhibited. Unloading part of the curve determines if it is elastic or plastic [see Figs. 12.3.1(a) and (b)]; the elastic material follows the same path in loading and unloading, while the plastic material shows a *history-dependent* path unloading.

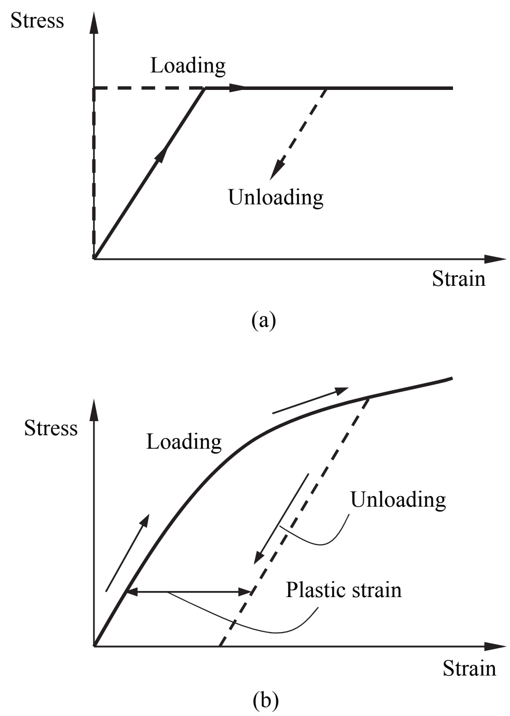

Fig. 12.3.1: Stress–strain behavior of (a) ideal plasticity and (b) strain-hardening plasticity.

The theory of plasticity deals with an analytical description of the stress–strain relations of a deformed body after a part or all of the body has yielded. The stress–strain relations must contain:

1. The elastic stress–strain relations.
2. The stress condition (or *yield criterion*) which indicates onset of yielding.
3. The stress–strain or stress–strain increment relations after the onset of plastic flow.

12.3.2 Ideal Plasticity

Many materials exhibit an ideal plastic (or elastic-perfectly-plastic) behavior, as shown in Fig. 12.3.1(a). In this case, there exists a limiting stress, called *yield stress*, denoted by σ_Y, at which the strains are indeterminate. For all stresses below the yield stress, a linear (or nonlinear) stress–strain relation is assumed:

$$\begin{aligned} &\sigma_{ij} < \sigma_Y \text{ linear elastic behavior} \\ &\sigma_{ij} \geq \sigma_Y \text{ plastic deformation (not recoverable)} \end{aligned} \tag{12.3.1}$$

12.3.3 Strain-Hardening Plasticity

A hardening plastic material model provides a refinement of the ideal plastic material model. In this model, it is assumed that the yield stress depends on some parameter κ (e.g. plastic strain ε^p), called the *hardening parameter*. The general yield criterion is expressed in the form

$$F(\sigma_{ij}, \kappa) = 0 \tag{12.3.2}$$

This yield criterion can be viewed as a surface in the stress space, with the position of the surface dependent on the instantaneous value of the hardening parameter κ. Since any yield criterion should be independent of the orientation of the coordinate system used, F should be a function of the stress invariants only. Experimental observations indicate that plastic deformation in metals is independent of hydrostatic pressure. Therefore, F must be a function of the stress invariants of the deviatoric stress tensor σ':

$$F(J_2', J_3', \kappa) = 0, \quad J_2' = \frac{1}{2}\sigma_{ij}'\sigma_{ij}', \quad J_3' = \frac{1}{3}\sigma_{ij}'\sigma_{jk}'\sigma_{ki}' \tag{12.3.3}$$

Two of the most commonly used yield criteria are given next.

The Tresca yield criterion

$$F = 2\bar{\sigma}\cos\theta - Y(\kappa) = 0, \quad \bar{\sigma} = \sqrt{J_2'} \tag{12.3.4}$$

The Huber–von Mises yield criterion

$$F = \sqrt{3J_2'} - Y(\kappa) = 0 \tag{12.3.5}$$

where Y is the yield stress from uniaxial tests, θ is the angle between the line of pure shear and the principal stress σ_1, and $\bar{\sigma} = \sqrt{J_2'}$ is called the *effective stress*.

After initial yielding, the stress level at which further plastic deformation occurs may be dependent on the current degree of plastic straining, known as *strain hardening*. Thus, the yield surface will vary (i.e. expand) at each stage of plastic deformation. When the yield surface is independent of the degree of plasticity, the material is said to be ideally (or perfectly) plastic. If the subsequent yield surfaces are a uniform expansion of the original yield surface, the hardening model is said to be *isotropic*. On the other hand, if the subsequent yield surfaces preserve their shape and orientation but translate in the stress space, *kinematic hardening* is said to take place.

Consider the uniaxial stress–strain curve shown in Fig. 12.3.2. The behavior is initially linear elastic with slope E (Young's modulus) until onset of yielding at the uniaxial yield stress σ_Y. Thereafter, the material response is elastic–plastic with the local tangent to the curve, E_T, called the elastic–plastic tangent modulus, continually changing.

At some stress level σ in the plastic range, if the load is increased to induce a stress of $d\sigma$, it results in a corresponding strain $d\varepsilon$. This increment of strain contains two parts: elastic $d\varepsilon^e$ (recoverable) and plastic $d\varepsilon^p$ (non-recoverable):

$$d\varepsilon = d\varepsilon^e + d\varepsilon^p, \quad d\varepsilon^e = \frac{d\sigma}{E}, \quad \frac{d\sigma}{d\varepsilon} = E_T \tag{12.3.6}$$

The strain-hardening parameter, H, is defined by

$$H = \frac{d\sigma}{d\varepsilon^p} = \frac{\frac{d\sigma}{d\varepsilon}}{1 - \frac{d\varepsilon^e}{d\varepsilon}} = \frac{E_T}{1 - \frac{E_T}{E}} \tag{12.3.7}$$

The element stiffness for the linear elastic portion is, say $\mathbf{K}^e$:

$$\mathbf{K}^e = \int_{x_a}^{x_b} \mathbf{B}^{\mathrm{T}} \mathbf{D}^e \mathbf{B} \; dx \tag{12.3.8}$$

where $\mathbf{D}^e$ is the linear elasticity matrix ($D^e = E$ for the uniaxial case). When the element deforms plastically, $\mathbf{D}^e$ reflects the decreased stiffness. This is computed, for uniaxial material behavior, by the following procedure: The increment in load dF causes an incremental displacement du

$$du = h_e \, d\varepsilon = h_e \left(d\varepsilon^e + d\varepsilon^p\right), \quad dF = A \, d\sigma = A_e H \, d\varepsilon^p \tag{12.3.9}$$

where h_e is the length and A_e the area of cross-section of the element. The effective stiffness is

$$E^{ep} = \frac{dF}{du} = \frac{A_e H \, d\varepsilon^p}{h_e \left(d\varepsilon^e + d\varepsilon^p\right)} = \frac{E A_e}{h_e} \left[1 - \frac{E}{(E+H)}\right] \tag{12.3.10}$$

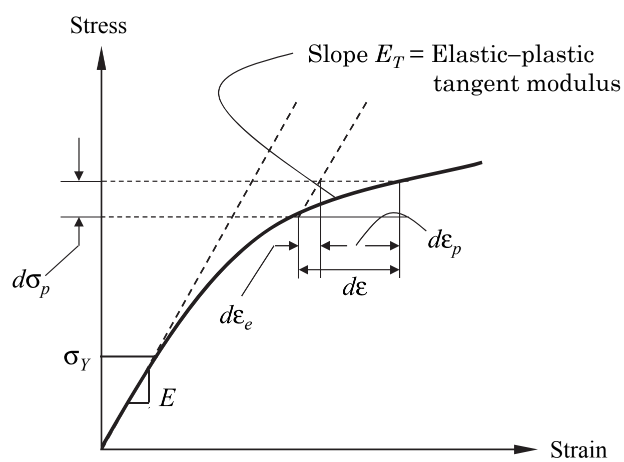

Fig. 12.3.2: A strain-hardening plastic behavior for the uniaxial case.

The element stiffness for the plastic range becomes,

$$\mathbf{K}^{ep} = \int_{x_a}^{x_b} \mathbf{B}^{\mathrm{T}} \mathbf{D}^{ep} \mathbf{B}\, dx \tag{12.3.11}$$

where $[D^{ep}]$ is the material stiffness in the plastic range. For uniaxial case $D^{ep} = E^{ep}$.

Equation (12.3.8) is valid when $\sigma < \sigma_Y$ and Eq. (12.3.11) is valid for $\sigma > \sigma_Y$. Note that $d\sigma = \sigma - \sigma_Y$ when $\sigma > \sigma_Y$.

12.3.4 Elastic–Plastic Analysis of a Bar

Here we present a detailed computational procedure for the analysis of an elastic–plastic problem. The procedure is described via a one-dimensional elastic–plastic bar problem. We shall consider a linear strain-hardening material subjected to an increasing uniaxial load.

12.3.4.1 Update of stresses

At a load-step number r where the deformation is elastic, the stress in a typical element with the strain increment $\Delta\varepsilon^r$ can be readily updated as

$$\sigma_i^r = \sigma_i^{(r-1)} + E_i \Delta\varepsilon^r \tag{12.3.12}$$

where E_i is the elastic modulus of element i. This linear elastic behavior will continue until a point where the resulting strain increment will initiate plastic yielding of the material. Now the updating of the stress in the element is not as straightforward as given in Eq. (12.3.12), and it can get complicated when the deformation is partly elastic and partly elastic–plastic, as shown from point A to point B in the stress–strain curve of Fig. 12.3.3.

To update the stress state from point A to point B, one can first assume that the deformation is elastic and compute the corresponding elastic stress, commonly referred to as the *elastic stress predictor*. Using Eq. (12.3.12), the elastic stress predictor σ_e can be calculated as

$$\sigma_{ei} = \sigma_i^{(r-1)} + E_i \Delta\varepsilon_i^r \quad \text{(no sum on } i) \tag{12.3.13}$$

Computing the elastic stress predictor brings the stress state from point A to point A′. A correction is made to transfer the stress state back to the elastic–plastic state at point B. We introduce a correction factor R (see Fig. 12.3.3)

$$R = \frac{\sigma_{ei} - \sigma_y}{\sigma_{ei} - \sigma_i^{(r-1)}} \tag{12.3.14}$$

so that the stress at point B can be written as

$$\sigma_i^r = \sigma_i^{(r-1)} + \left[(1-R)E_i + RE_T\right] \Delta\varepsilon_i^r \tag{12.3.15}$$

Here E_T denotes the elastic–plastic tangent modulus, which is related to the elastic modulus E and strain-hardening parameter H by Eq. (12.3.7). In the case where the element has already yielded in previous load steps, as illustrated by point C in Fig. 12.3.3, the approach of determining the elastic stress predictor and making correction to the stress state at point D still applies with $R = 1$ in Eq. (12.3.15):

$$\sigma_i^r = \sigma_i^{(r-1)} + E_T \Delta\varepsilon_i^r \tag{12.3.16}$$

12.3.4.2 Update of plastic strain

The extent of plastic flow in a deformed material can be readily characterized by the measure of plastic strain. To determine the plastic strain in an element at point B of Fig. 12.3.3, it will be useful to rewrite Eq. (12.3.15) as

$$\sigma_i^r = \sigma_Y + E_T(R\,\Delta\varepsilon_i^r) \equiv \sigma_Y + \Delta\sigma_i^r \tag{12.3.17}$$

Equation (12.3.17) can be interpreted as that adjusts the stress state at point A to the yield stress before predicting the elastic stress and its correction. This will allow one to isolate the stress component $\Delta\sigma_i^r$ and strain $R\,\Delta\varepsilon_i^r$ that are involved in the plastic flow. With Eq. (12.3.6), the plastic strain increment is

$$\Delta\varepsilon_{pi}^r = R\Delta\varepsilon_i^r - \frac{\Delta\sigma_i^r}{E_i} = \left(1 - \frac{E_T}{E_i}\right) R\,\Delta\varepsilon_i^r \tag{12.3.18}$$

Equation (12.3.18) can also be used for elements that have already yielded in previous load steps by setting $R = 1$.

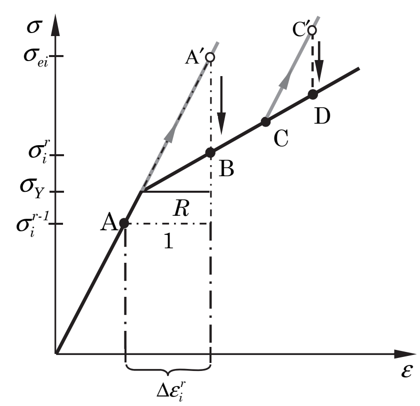

Fig. 12.3.3: Transition of elastic to elastic–plastic behavior.

12.3.4.3 Update of yield stress limit

Besides assessing the extent of plastic deformation, the measure of the plastic strain will become especially crucial for strain-hardening materials where the yield limit is a function of the plastic strain. A plot of yield limit against the plastic strain for a typical linear strain-hardening material is shown in Fig. 12.3.4. Once the plastic strain occurs, the yield limit will be modified and updated as

$$\sigma_{yi}^r = \sigma_Y + H\,\Delta\varepsilon_{pi}^r \tag{12.3.19}$$

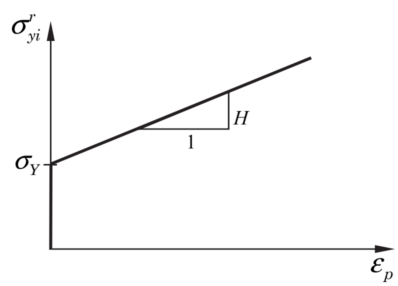

Fig. 12.3.4: Stress–strain behavior of a strain-hardening material.

12.3.4.4 Identification of deformation modes

The updated yield limit will come in handy when one is to check the type of deformation an element is undergoing. Once the correct type of deformation is identified, the stress and strain values can then be updated according to Eqs. (12.3.l5) and (12.3.18). There are four types of deformation:

(a) *Elastic Loading:* (an element that has not yielded previously continues to deform elastically)

$$|\sigma_i^{r-1}| < |\sigma_{yi}^{r-1}| \quad \text{and} \quad |\sigma_{ei}| < |\sigma_{yi}^{r-1}| \tag{12.3.20a}$$

(b) *Elastic–plastic Loading:* (an element that has not yielded previously will deform elastic–plastically)

$$|\sigma_i^{r-1}| < |\sigma_{yi}^{r-1}| \quad \text{and} \quad |\sigma_{ei}| > |\sigma_{yi}^{r-1}| \tag{12.3.20b}$$

(c) *Plastic Loading:* (an element that previously yielded will continue to deform plastically)

$$|\sigma_i^{r-1}| > |\sigma_{yi}^{r-1}| \quad \text{and} \quad |\sigma_{ei}| > |\sigma_i^{r-1}| \tag{12.3.20c}$$

(d) *Elastic Unloading:* (an element previously yielded is now unloading elastically)

$$|\sigma_i^{r-1}| > |\sigma_{yi}^{r-1}| \quad \text{and} \quad |\sigma_{ei}| < |\sigma_i^{r-1}| \tag{12.3.20d}$$

12.3.4.5 Force equilibrium

Since the displacement finite element model is based on the principle of virtual displacements, the solution satisfies the equilibrium equations, provided the deformation is linearly elastic. However, in the finite element analysis of elastic–plastic problems equilibrium equations may not be satisfied during the period when stresses are adjusted to account for plastic strains. Adjustments must be made to achieve equilibrium at each step by redistributing the forces neighboring elements.

For example, consider a node N at the interface of element i that has yielded and the adjacent element $i+1$ that is still elastic (see Fig. 12.3.5). At this node, the force equilibrium will be violated during the analysis because the force in element i is limited such that the stress in the element does not exceed the yield stress. The difference between the force calculated using the elastic analysis and the plastic force must now be taken up by all other elastic elements in the mesh. Thus to restore equilibrium of forces, a force correction must be made at the node N:

$$\Delta F = F_i - F_{i+1} - F_N \tag{12.3.21}$$

However, to preserve the finite element equations of the original problem (to retain the same forces in other unaffected elements), the force correction cannot be imposed as a nodal force. Instead, the force correction may be applied as a nodal displacement

$$\Delta u_N^c = \frac{\Delta F\, L_i}{E_T A_i} \tag{12.3.22}$$

where L_i and A_i are the length and cross-sectional area of element i. This correction procedure will continue until force equilibrium at all nodes is restored, within an acceptable error of tolerance. Figure 12.3.6 contains the flow chart of various steps in the elastic–plastic analysis of a typical problem.

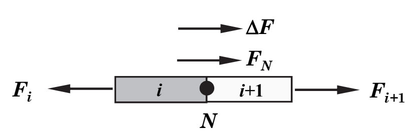

Fig. 12.3.5: Force equilibrium at node N.

12.3.4.6 A numerical example

Consider a bar of length 5 m that is fixed at one end and is subjected to a uniform body force f. The material properties of the bar are taken as

$$E = 10^4 \text{ N/m}^2, \quad A = 1 \text{ m}^2, \quad \sigma_y = 5 \text{ N/m}^2, \quad H = 10^3 \text{ N/m}^2$$

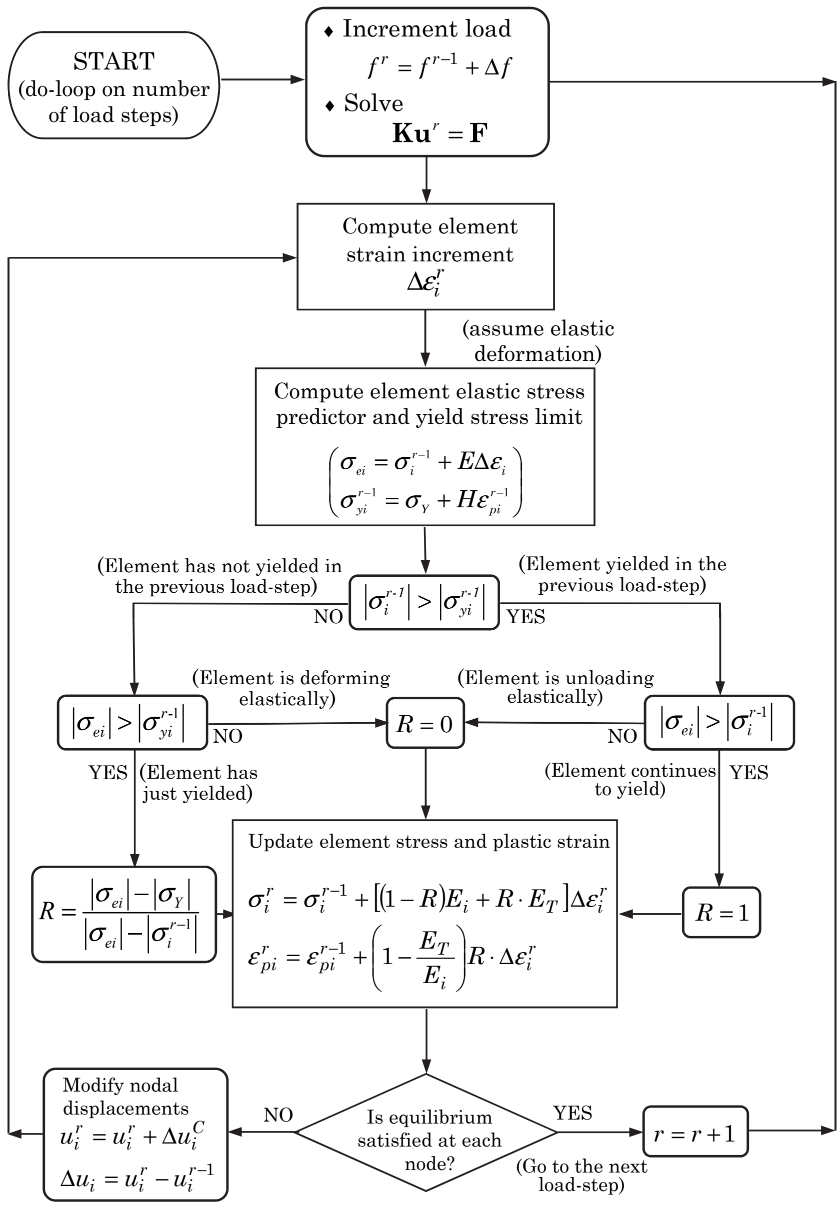

Fig. 12.3.6: Flow chart for elastic–plastic analysis of a bar.

The bar is discretized using a mesh of five linear elements. The elastic–plastic iterative scheme discussed in this section was implemented and the results are presented in Tables 12.3.1 and 12.3.2. At the start of the analysis when elements are still elastic, a nominal body force of 0.005 N/m was imposed to find the maximum stress induced in the elements. The critical load F_{cr} for

Table 12.3.1: Nodal displacements for various load steps.

Body force f	Node no.	Nodal displacement*
0.0050	2	2.2500×10^{-6}
	3	4.0000×10^{-6}
	4	5.2500×10^{-6}
	5	6.0000×10^{-6}
	6	6.2500×10^{-6}
1.1111	2	5.0000×10^{-4}
	3	8.8889×10^{-4}
	4	1.1667×10^{-3}
	5	1.3333×10^{-3}
	6	1.3889×10^{-3}
1.1161	2	5.2475×10^{-4} (5.2475×10^{-4})
	3	9.1539×10^{-4} (9.1539×10^{-4})
	4	1.1944×10^{-3} (1.1944×10^{-3})
	5	1.3618×10^{-3} (1.3618×10^{-3})
	6	1.4176×10^{-3} (1.4176×10^{-3})
10.0050	2	4.9525×10^{-2} (4.4525×10^{-2})
	3	8.8044×10^{-2} (7.8044×10^{-2})
	4	1.1556×10^{-1} (1.0056×10^{-1})
	5	1.3207×10^{-1} (1.1207×10^{-1})
	6	1.3257×10^{-1} (1.1257×10^{-1})

* Values in parentheses are corrected to satisfy force equilibrium at each node.

the first element to yield was computed from this maximum element stress and is imposed in the next load-step:

$$F_{\rm cr} = \frac{\sigma_Y f}{\max|\sigma_i|}, \qquad i = 1, 2, \cdots, N \tag{12.3.23}$$

Here i is the element number and N is the total number of un-yielded elements. In the new load-step where f is 1.1111 N/m, the computed results reveal that the first element (element 1 in this example) had just yielded; up to this point, the analysis is still elastic. Then another nominal body force of 0.005 N/m is added to calculate the critical load for the next element to yield. The stiffness of the yielded Element 1 is reduced in this load-step and the results in Table 12.3.2 indicate a violation of force equilibrium at the nodes connecting the yielded element, except for the node that is fixed. Corrections to the nodal displacements were made until equilibrium was satisfied at all nodes. Only then, the critical load for the next element to yield could be calculated and the

Table 12.3.2: Element stresses and strains for various load steps.

Body force f	Element number	Total strain ε	Plastic strain ε_p	Bar force $\lvert F\rvert = \sigma A$
0.0050	1	2.2500×10^{-6}	0	0.0225
	2	1.7500×10^{-6}	0	0.0175
	3	1.2500×10^{-6}	0	0.0125
	4	0.7500×10^{-6}	0	0.0075
	5	0.2500×10^{-6}	0	0.0025
1.1111	1*	5.0000×10^{-4}	0	5.0000
	2	3.8889×10^{-4}	0	3.8889
	3	2.7778×10^{-4}	0	2.7778
	4	1.6667×10^{-4}	0	1.6667
	5	0.5556×10^{-4}	0	0.5556
1.1161	1	5.5248×10^{-4}	4.5680×10^{-3}	9.5680
	2	3.9064×10^{-4}	0	3.9064
	3	2.7903×10^{-4}	0	2.7903
	4	1.6742×10^{-4}	0	1.6742
	5	0.5581×10^{-4}	0	0.5581
Corrected	1	5.2475×10^{-4}	0.2250×10^{-4}	5.0225
to satisfy	2	3.9064×10^{-4}	0	3.9064
force	3	2.7903×10^{-4}	0	2.7903
equilibrium	4	1.6742×10^{-4}	0	1.6742
	5	0.5581×10^{-4}	0	0.5581
...	...	...	...	...
10.0050	1	4.9525×10^{-2}	4.4568×10^{-2}	49.5680
	2	3.8519×10^{-2}	3.4563×10^{-2}	39.5630
	3	2.7514×10^{-2}	2.4558×10^{-2}	29.5580
	4	1.6508×10^{-2}	1.4553×10^{-2}	19.5530
	5	0.5503×10^{-2}	0.4548×10^{-2}	9.5480
Corrected	1	4.4525×10^{-2}	4.0023×10^{-2}	45.0225
to satisfy	2	3.3519×10^{-2}	3.0018×10^{-2}	35.0175
force	3	2.2514×10^{-2}	2.0013×10^{-2}	25.0125
equilibrium	4	1.1508×10^{-2}	1.0008×10^{-2}	15.0075
	5	5.0275×10^{-4}	0.0025×10^{-4}	5.0025

* Element just yielded at that load step.

procedure is repeated until all elements yield. Reaction forces at the fixed end of the bar against the free-end displacements are plotted in Fig. 12.3.7, together with the results from the commercial finite element software ABAQUS. There is a very good agreement with the solutions generated by the iterative scheme discussed and those obtained with ABAQUS. A 20-element mesh also produced results identical to those in Fig. 12.3.7; the results are also verified using ABAQUS. Figure 12.3.8 contains the true stress–strain diagram of Element 1, where one may note that the elastic–plastic material curve is recovered.

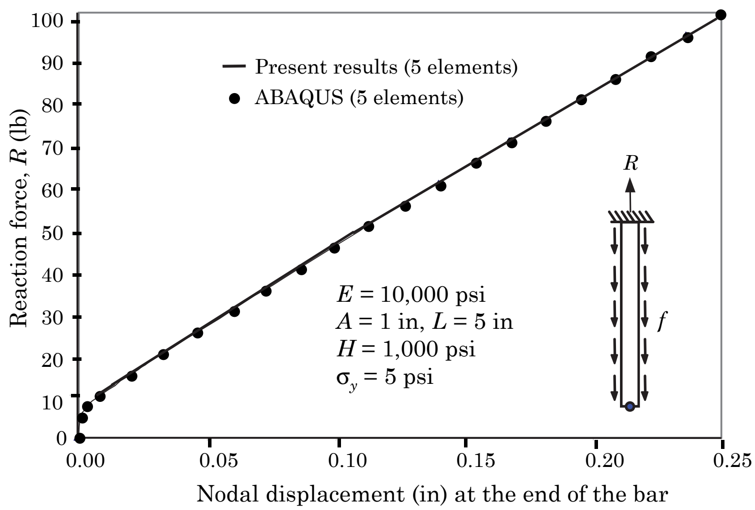

Fig. 12.3.7: Reaction forces versus nodal displacements at bar end.

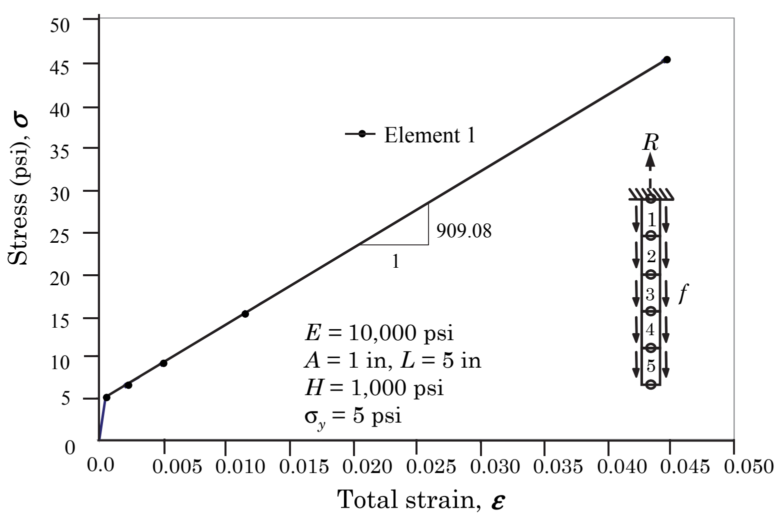

Fig. 12.3.8: True stress–strain curve of Element 1.

This completes a discussion of the elastic–plastic finite element models of one-dimensional problems. Extension of the ideas discussed here can be extended to beams and plates. The book by Owen and Hinton [289] provides the necessary theoretical formulations and computer programs for interested readers (also see [290]).

12.4 Nonlinear Viscoelastic Analysis of the Euler–Bernoulli and Timoshenko Beams

12.4.1 Introduction

There are many engineering materials that cannot be adequately modeled using the classical elasticity formulation. One category of such materials is the set of viscoelastic materials, examples of which include polymers, concrete structures and metals at elevated temperatures. The theoretical foundations for viscoelasticity are well established [3, 291–295]. Analytical methods have been employed successfully in the study of the mechanical response of viscoelastic continua. The Laplace transform method was employed by Flügge [291] in the analysis of viscoelastic beams. The correspondence principle has also been used by Christensen [292] and Findley, Lai, and Onaran [296] to convert linear elasticity solutions into viscoelasticity solutions through the use of integral transformations [3]. Analytical solutions based on the Laplace transform method or correspondence principle, however, are limited to linear problems with very simple geometric configurations, boundary conditions, and material models.

Numerical methods provide a powerful framework for obtaining approximate solutions to viscoelasticity problems. In particular, the finite element method has been employed successfully in the analysis of viscoelastic bodies by many researchers. Taylor, Pister, and Goudreau [297] used the finite element method in conjunction with a recurrence relation to solve viscoelasticity problems such that data from only the previous time step (as opposed to the entire deformation history) is needed in determining a body's configuration at the current time step. Oden and Armstrong [298] developed a finite element framework for thermoviscoelasticity and presented numerical solutions to thick-walled cylinder problems with time-dependent boundary conditions. In their work, they extended the recurrence formulation to nonlinear problems. Additional general finite element formulations for viscoelastic continua can be found in [299–302].

Although three-dimensional finite element formulations are applicable to continua in general, it is often computationally advantageous to specialize these models to structural elements such as beams, plates, and shells. There are a variety of finite element models in the literature for viscoelastic beams. Most of these models employ some form of either the Euler–Bernoulli or Timoshenko beam theories. The major challenges encountered in any viscoelastic finite element formulation are due to the viscoelastic constitutive equations, often expressed in convolution form. Rencis, Saigal, and Jong [303] presented a simple Euler–Bernoulli beam finite element model using an incremental approach. In their analysis, the viscoelastic convolution integrals are replaced by creep strain increments in the form of fictitious body forces.

The Laplace transform approach has been employed by several researchers [304–306] in conjunction with the finite element method. Chen [304] successfully analyzed viscoelastic Timoshenko beams by converting the time-dependent and convolution form of the finite element equations into a set of algebraic equations in s space. The solution in the time domain was determined through a numerical inversion of the Laplace transform. In his analysis, Chen assumed that the Poisson ratio is constant. This assumption is consistent with the findings of Zheng-you, Gen-guo, and Chang-jun [307], who presented analytical solutions for Timoshenko beams with time-dependent and time-independent Poisson's ratios. Aköz and Kadioğlu [305] presented two Timoshenko beam finite elements using the Laplace–Carson method and a mixed formulation. As in the work by Chen [304], the finite element formulations require numerical inversion from the Laplace–Carson domain back to the time domain. Temel, Calim, and Tütüncü [306] studied the viscoelastic deformation of cylindrical helical rods using the Timoshenko beam hypotheses. Solutions obtained in the Laplace domain were transformed to the time domain through the inverse Laplace transform method.

The Fourier transform method has also been used in the finite element formulation of viscoelastic beams. Chen and Chan [308] developed finite element formulations for beams, plates, and shells, and used the Fourier transform approach to reduce the time dependent formulations into equations in the frequency domain for generalized eigenvalues.

The anelastic displacement formulation (ADN) has also been employed in the analysis of viscoelastic beams. Trindade, Benjeddou, and Ohayon [309] used the ADN approach in the analysis of sandwich beams with viscoelastic cores. In their formulation, they employed the Euler–Bernoulli beam theory for the outer faces and the Timoshenko beam theory for the inner viscoelastic core. Pálfalvi [310] also employed the ADN formulation in the analysis of viscoelastic Euler–Bernoulli beams.

An additional method for circumventing challenges associated with the convolution integral is the Golla–Hughes–McTavish (GHM) method. The method is described in the publications by McTavish and Hughes [311, 312]. In the GHM method, the Laplace transform approach is used to convert the viscoelastic time-dependent equations into the Laplace domain. An auxiliary coordinate (or dissipation coordinate) is also introduced. The equations are then converted into an equivalent set of equations in the time domain that bears a standard dynamics form without any convolution integrals. The GHM method was used successfully by Balamurugan and Narayanan [313, 314] in the transient finite element analysis of Timoshenko beams possessing viscoelastic layers.

It has been noted that when the relaxation moduli can be expressed as a Prony series, the linear viscoelastic constitutive equations in convolution form can be expressed as an equivalent set of ordinary differential equations in terms of a collection of internal strain variables. Johnson, Tessler, and Dambach [315] applied this approach to the analysis of high-order viscoelastic beams where the effects of shear deformation and transverse extensions were included in the formulation. This method has also been employed by Austin and Inman [316].

Finite element formulations for Euler–Bernoulli and Timoshenko beams have also been formulated using the fractional derivative viscoelastic constitutive model by Galucio, Deü, and Ohayon, [317] in the analysis of sandwich beam structures. Ranzi and Zona [318] analyzed a composite steel–concrete beam structure via the finite element method using an elastic formulation for the steel and a viscoelastic constitutive relation for the concrete. The Timoshenko beam theory was used for the steel and Euler–Bernoulli beam theory for the concrete. In their formulation, the trapezoidal rule was employed to replace the convolution integral with a summation of quantities.

The viscoelastic beam finite element formulations reviewed above are restricted to infinitesimal strain and small deformation analysis. As a result, these models are unable to account for nonlinear geometric effects that can be significant when loads are sufficiently large. Recently, Payette and Reddy [319, 320], Vallala, Payette, and Reddy [321], and Vallala, Ruimi, and Reddy [322] presented quasi-static finite element formulations for Euler–Bernoulli (EBT), Timoshenko (TBT), and Reddy (RBT) beam theories with linear viscoelastic material properties.

In this section, following the work of Payette and Reddy [319], weak-form finite element models for the nonlinear quasi-static analysis of initially straight viscoelastic Euler–Bernoulli and Timoshenko beams are presented using the principle of virtual work. The mechanical properties of the beams are considered to be linear viscoelastic. However, large transverse displacements, moderate rotations, and small strains are allowed by retaining the *von Kármán* strain components of the simplified Green–Lagrange strain tensor in the formulation. The fully-discretized finite element equations are developed using the trapezoidal rule in conjunction with a two-point recurrence relation. The resulting finite element equations, therefore, necessitate data storage from the previous time step only, and not the entire deformation history. Membrane locking is eliminated from the Euler–Bernoulli formulation through the use of selective reduced Gauss–Legendre quadrature. Membrane and shear locking are both circumvented in the Timoshenko beam finite element by employing a family of high-order Lagrange polynomials. A Newton iterative scheme is used to solve the nonlinear finite element equations.

12.4.2 Governing Equations

12.4.2.1 Displacement and strain fields

There are a number of theories that are used to represent the kinematics for the deflection of beams (see Reddy [323] for a review of the beam theories), and two of them, namely, the Euler–Bernoulli beam theory (EBT) and the Timoshenko beam theory (TBT), were discussed in detail in Chapter 5. For the sake of ready reference, here we review the kinematics of the two beam theories.

The Euler–Bernoulli beam theory is based on the following displacement field:

$$\begin{aligned} u_1(x,z,t) &= u(x,t) - z\frac{\partial w}{\partial x} \\ u_3(x,z,t) &= w(x,t) \end{aligned} \tag{12.4.1}$$

where u is the axial deflection of the mid-plane $(x,0)$ of the beam, and w represents the transverse deflection of the mid-plane. The x-coordinate is taken along the beam length, and the z-coordinate along the thickness direction of the beam. Deformation is therefore confined to the xz-plane. The Euler–Bernoulli displacement field implies that straight lines orthogonal to the mid-surface before deformation remain so after deformation. The nonzero strain component for the Euler–Bernoulli beam theory can be expressed as

$$\varepsilon_{xx} = \frac{\partial u}{\partial x} + \frac{1}{2}\left(\frac{\partial w}{\partial x}\right)^2 - z\frac{\partial^2 w}{\partial x^2} \tag{12.4.2}$$

The Timoshenko beam theory is based on the displacement field

$$\begin{aligned} u_1(x,z,t) &= u(x,t) + z\phi_x(x,t) \\ u_3(x,z,t) &= w(x,t) \end{aligned} \tag{12.4.3}$$

where ϕ_x denotes the rotation of a transverse normal about the y axis. The nonzero strain components for the Timoshenko theory are

$$\begin{aligned} \varepsilon_{xx} &= \frac{\partial u}{\partial x} + \frac{1}{2}\left(\frac{\partial w}{\partial x}\right)^2 + z\frac{\partial \phi_x}{\partial x} \\ \gamma_{xz} &= \phi_x + \frac{\partial w}{\partial x} \end{aligned} \tag{12.4.4}$$

12.4.2.2 Linear viscoelastic constitutive equations

For linear viscoelastic materials, the one-dimensional constitutive equations relating the components of the second Piola–Kirchhoff stress tensor $\boldsymbol{\sigma}$ and the Green–Lagrange strain tensor $\boldsymbol{\varepsilon}$ may be expressed in the following integral forms:

$$\sigma_{xx}(\mathbf{x},t) = E(0)\,\varepsilon_{xx}(\mathbf{x},t) + \int_0^t \dot{E}(t-s)\,\varepsilon_{xx}(\mathbf{x},s)\,ds \tag{12.4.5}$$

$$\sigma_{xz}(\mathbf{x},t) = G(0)\,\gamma_{xz}(\mathbf{x},t) + \int_0^t \dot{G}(t-s)\,\gamma_{xz}(\mathbf{x},s)\,ds \tag{12.4.6}$$

where $E(t)$ and $G(t)$ are the relaxation moduli. The specific forms of $E(t)$ and $G(t)$ will in general depend upon the material model employed. For the present analysis we assume that $E(t)$ and $G(t)$ can be expressed in terms of a Prony series of order n as

$$E(t) = E_0 + \sum_{i=1}^{n} E_i e^{-\frac{t}{\tau_i^E}}, \qquad G(t) = G_0 + \sum_{i=1}^{n} G_i e^{-\frac{t}{\tau_i^G}} \tag{12.4.7}$$

It is important to note that the integral constitutive equations given in Eqs. (12.4.5) and (12.4.6) above are only valid for materials with bounded creep response. In addition the present constitutive models assume that a discontinuity exits in the response only at $t = 0$.

12.4.3 Weak Forms

The finite element models of the Euler–Bernoulli and Timoshenko beam theories in the present work are developed by applying the principle of virtual work (or principle of virtual displacements) to a typical beam finite element. In our finite element formulation we discretize the computational domain $\Omega = [0, L]$ into a set of N non-overlapping subdomains $\Omega^e = [x_a^e, x_b^e]$, such that $\Omega = \bigcup_{e=1}^{N} \Omega^e$. The quasi-static form of the virtual work expression can be expressed over the volume $V^e = A^e \times \Omega^e$ of a typical finite element as

$$\int_{x_a^e}^{x_b^e} \int_{A^e} (\delta\boldsymbol{\varepsilon} : \boldsymbol{\sigma} - \delta\mathbf{u} \cdot \mathbf{f})\, dA dx - \oint_{\Gamma^e} \delta\mathbf{u} \cdot \mathbf{t}\, ds = 0 \tag{12.4.8}$$

where A^e is the cross-sectional area of a typical beam element, $\Gamma^e = \partial V^e$ and δ is the variational operator. The additional quantities $\mathbf{f}$ and $\mathbf{t}$ are the body force and traction vectors, respectively. Equation (12.4.8) is the weak form of the classical Euler equations of motion for a continuous body. It is this expression that will be used in the development of our finite element models for each beam theory.

12.4.3.1 The Euler–Bernoulli beam theory

The virtual work principle results in the weak forms of the Euler–Bernoulli beam equations. The variational problem for the EBT is to find $(u, w) \in H^1(\Omega^e) \times H^2(\Omega^e)$ for all $(\delta u, \delta w) \in H^1(\Omega^e) \times H^2(\Omega^e)$, where $H^m(\Omega^e)$ is the Hilbert space of order m, such that

$$0 = \int_{x_a}^{x_b} \left(\frac{\partial \delta u}{\partial x} N_{xx} - f \delta u \right) dx - Q_1 \delta u(x_a) - Q_4 \delta u(x_b) \tag{12.4.9}$$

$$\begin{aligned} 0 = \int_{x_a}^{x_b} \left(\frac{\partial \delta w}{\partial x} \frac{\partial w}{\partial x} N_{xx} - \frac{\partial^2 \delta w}{\partial x^2} M_{xx} - q \delta w \right) dx - Q_2 \delta w(x_a) \\ - Q_3 \left(-\frac{\partial \delta w}{\partial x} \right)\bigg|_{x=x_a} - Q_5 \delta w(x_b) - Q_6 \left(-\frac{\partial \delta w}{\partial x} \right)\bigg|_{x=x_b} \end{aligned} \tag{12.4.10}$$

where Q_j are the generalized nodal forces. In Eqs. (12.4.9) and (12.4.10) and throughout the rest of this section, f and q are distributed axial and transverse loads, respectively. In addition, A is the cross-sectional area and I is the moment of inertia. For the sake of brevity we have dropped superscripts e from quantities in the above equations and throughout the remainder of this work. The internal normal force N_{xx} and bending moment M_{xx} in the above equations can be expressed in terms of the displacements using the viscoelastic constitutive relations as

$$\begin{aligned} N_{xx} &= E(0)\,A\left[\frac{\partial u}{\partial x} + \frac{1}{2}\left(\frac{\partial w}{\partial x}\right)^2\right] \\ &\quad + \int_0^t \dot{E}(t-s)\,A\left[\frac{\partial u(x,s)}{\partial x} + \frac{1}{2}\left(\frac{\partial w(x,s)}{\partial x}\right)^2\right] ds \end{aligned} \tag{12.4.11}$$

$$\begin{aligned} M_{xx} &= -E(0)\,I\frac{\partial^2 w}{\partial x^2} \\ &\quad - \int_0^t \dot{E}(t-s)\,I\frac{\partial^2 w(x,s)}{\partial x^2} ds \end{aligned} \tag{12.4.12}$$

12.4.3.2 The Timoshenko beam theory

For the Timoshenko beam theory, the variational or weak form problem is to find $(u, w, \phi_x) \in H^1(\Omega^e) \times H^1(\Omega^e) \times H^1(\Omega^e)$ for all $(\delta u, \delta w, \delta\phi_x) \in H^1(\Omega^e) \times H^1(\Omega^e) \times H^1(\Omega^e)$ such that

$$0 = \int_{x_a}^{x_b} \left(\frac{\partial \delta u}{\partial x} N_{xx} - \delta u\, f\right) dx - Q_1 \delta u(x_a) - Q_4 \delta u(x_b) \tag{12.4.13}$$

$$\begin{aligned} 0 &= \int_{x_a}^{x_b} \left(\frac{\partial \delta w}{\partial x}\frac{\partial w}{\partial x} N_{xx} + \frac{\partial \delta w}{\partial x} Q_x - \delta w\, q\right) dx \\ &\quad - Q_2 \delta w(x_a) - Q_5 \delta w(x_b) \end{aligned} \tag{12.4.14}$$

$$0 = \int_{x_a}^{x_b} \left(\frac{\partial \delta\phi_x}{\partial x} M_{xx} + \delta\phi_x Q_x\right) dx - Q_3 \delta\phi_x(x_a) - Q_6 \delta\phi_x(x_b) \tag{12.4.15}$$

In addition to the normal force N_{xx} and bending moment M_{xx}, the TBT also admits a transverse shear force Q_x. For the Timoshenko formulation, the internal reactions can be expressed in terms of the generalized displacement components as

$$\begin{aligned} N_{xx} &= E(0)\,A\left[\frac{\partial u}{\partial x} + \frac{1}{2}\left(\frac{\partial w}{\partial x}\right)^2\right] \\ &\quad + \int_0^t \dot{E}(t-s)\,A\left[\frac{\partial u(x,s)}{\partial x} + \frac{1}{2}\left(\frac{\partial w(x,s)}{\partial x}\right)^2\right] ds \end{aligned} \tag{12.4.16}$$

$$M_{xx} = E(0)\, I \frac{\partial \phi_x}{\partial x} + \int_0^t \dot{E}(t-s)\, I \frac{\partial \phi_x(x,s)}{\partial x} ds \tag{12.4.17}$$

$$\begin{aligned} Q_x &= K_s G(0)\, A \left(\phi_x + \frac{\partial w}{\partial x} \right) \\ &\quad + \int_0^t K_s \dot{G}(t-s)\, A \left(\phi_x(x,s) + \frac{\partial w(x,s)}{\partial x} \right) ds \end{aligned} \tag{12.4.18}$$

where K_s is the shear correction coefficient. This factor equates the shear energy present in the TBT with what is calculated from the equilibrium equations of elasticity. The quantities Q_j are the generalized nodal forces in the Timoshenko beam finite element.

12.4.4 Semi-Discrete Finite Element Models

In this section we present the semi-discrete finite element models for the classical and shear deformable beam theories. For each beam finite element formulation the resulting nonlinear semi-discrete equations can be expressed in matrix form as

$$\mathbf{K}\boldsymbol{\Delta} + \int_0^t \tilde{\mathbf{K}}\boldsymbol{\Delta}(s)\, ds = \mathbf{F} \tag{12.4.19}$$

For each beam finite element formulation the matrices in Eq. (12.4.19) can be expressed in the following partitioned forms:

$$\mathbf{K} = \begin{bmatrix} \mathbf{K}^{11} & \cdots & \mathbf{K}^{1\alpha} \\ \vdots & \ddots & \vdots \\ \mathbf{K}^{\alpha 1} & \cdots & \mathbf{K}^{\alpha\alpha} \end{bmatrix}, \quad \tilde{\mathbf{K}} = \begin{bmatrix} \tilde{\mathbf{K}}^{11} & \cdots & \tilde{\mathbf{K}}^{1\alpha} \\ \vdots & \ddots & \vdots \\ \tilde{\mathbf{K}}^{\alpha 1} & \cdots & \tilde{\mathbf{K}}^{\alpha\alpha} \end{bmatrix} \tag{12.4.20}$$

$$\boldsymbol{\Delta} = \left\{ (\boldsymbol{\Delta}^1)^{\mathrm{T}} \cdots (\boldsymbol{\Delta}^\alpha)^{\mathrm{T}} \right\}^{\mathrm{T}}, \quad \mathbf{F} = \left\{ (\mathbf{F}^1)^{\mathrm{T}} \cdots (\mathbf{F}^\alpha)^{\mathrm{T}} \right\}^{\mathrm{T}} \tag{12.4.21}$$

where $\alpha = 2$ for the Euler–Bernoulli beam theory and $\alpha = 3$ for the Timoshenko beam theory.

12.4.4.1 The Euler–Bernoulli beam finite element

For the EBT finite element model we introduce the following interpolation scheme of the displacement field variables

$$u(x,t) = \sum_{j=1}^{2} \Delta_j^1(t)\, \psi_j^{(1)}(x), \qquad w(x,t) = \sum_{j=1}^{4} \Delta_j^2(t)\, \psi_j^{(2)}(x) \tag{12.4.22}$$

where Δ_j^1 and Δ_j^2 are the generalized displacements at the nodes and $\psi_j^{(1)} \in H^1(\Omega^e)$ and $\psi_j^{(2)} \in H^2(\Omega^e)$ are the linear Lagrange and Hermite cubic interpolation functions, respectively. The interpolation functions can be expressed with respect to the natural coordinate

$$\xi = \frac{2\left(x - x_a\right)}{h_x} - 1 \tag{12.4.23}$$

as

$$\psi_1^{(1)} = \frac{1}{2}\left(1 - \xi\right), \qquad \psi_2^{(1)} = \frac{1}{2}\left(1 + \xi\right) \tag{12.4.24}$$

$$\begin{aligned} \psi_1^{(2)} &= \frac{1}{4}\left(\xi - 1\right)^2\left(\xi + 2\right), & \psi_2^{(2)} &= -\frac{h_x}{8}\left(\xi - 1\right)^2\left(\xi + 1\right) \\ \psi_3^{(2)} &= -\frac{1}{4}\left(\xi + 1\right)^2\left(\xi - 2\right), & \psi_4^{(2)} &= -\frac{h_x}{8}\left(\xi + 1\right)^2\left(\xi - 1\right) \end{aligned} \tag{12.4.25}$$

In the above equations and throughout the rest of this paper, $h_x = x_b - x_a$ is the length of a given finite element. Inserting Eq. (12.4.22) into Eqs. (12.4.9) and (12.4.10) results in the semi-discrete finite element equations for the Euler–Bernoulli beam theory. The resulting matrices can be determined by the following formulae [compare with Eq. (5.2.31)]:

$$\begin{aligned} K_{ij}^{11} &= \int_{x_a}^{x_b} E\left(0\right) A \frac{d\psi_i^{(1)}}{dx}\frac{d\psi_j^{(1)}}{dx} dx \\ K_{ij}^{12} &= \frac{1}{2} K_{ji}^{21} = \frac{1}{2}\int_{x_a}^{x_b} \left(E\left(0\right) A \frac{\partial w}{\partial x}\right) \frac{d\psi_i^{(1)}}{dx}\frac{d\psi_j^{(2)}}{dx} dx \\ K_{ij}^{22} &= \int_{x_a}^{x_b} E\left(0\right) I \frac{d^2\psi_i^{(2)}}{dx^2}\frac{d^2\psi_j^{(2)}}{dx^2} dx \\ &\quad + \frac{1}{2}\int_{x_a}^{x_b} \left[E\left(0\right) A \left(\frac{\partial w}{\partial x}\right)^2\right] \frac{d\psi_i^{(2)}}{dx}\frac{d\psi_j^{(2)}}{dx} dx \\ \tilde{K}_{ij}^{11} &= \int_{x_a}^{x_b} \dot{E}\left(t - s\right) A \frac{d\psi_i^{(1)}}{dx}\frac{d\psi_j^{(1)}}{dx} dx \\ \tilde{K}_{ij}^{12} &= \frac{1}{2}\int_{x_a}^{x_b} \left(\dot{E}\left(t - s\right) A \frac{\partial w\left(x, s\right)}{\partial x}\right) \frac{d\psi_i^{(1)}}{dx}\frac{d\psi_j^{(2)}}{dx} dx \\ \tilde{K}_{ij}^{21} &= \int_{x_a}^{x_b} \left(\dot{E}\left(t - s\right) A \frac{\partial w\left(x, s\right)}{\partial x}\right) \frac{d\psi_i^{(2)}}{dx}\frac{d\psi_j^{(1)}}{dx} dx \\ \tilde{K}_{ij}^{22} &= \int_{x_a}^{x_b} \dot{E}\left(t - s\right) I \frac{d^2\psi_i^{(2)}}{dx^2}\frac{d^2\psi_j^{(2)}}{dx^2} dx \\ &\quad + \frac{1}{2}\int_{x_a}^{x_b} \left(\dot{E}\left(t - s\right) A \frac{\partial w}{\partial x}\frac{\partial w\left(x, s\right)}{\partial x}\right) \frac{d\psi_i^{(2)}}{dx}\frac{d\psi_j^{(2)}}{dx} dx \end{aligned} \tag{12.4.26}$$

$$
\begin{aligned}
F_i^1 &= \int_{x_a}^{x_b} f\psi_i^{(1)} dx + Q_1\psi_i^{(1)}(x_a) + Q_4\psi_i^{(1)}(x_b) \\
F_i^2 &= \int_{x_a}^{x_b} q\,\psi_i^{(2)} dx + Q_2\psi_i^{(2)}(x_a) + Q_5\psi_i^{(2)}(x_b) \\
&\quad + Q_3\left(-\frac{\partial\psi_i^{(2)}}{\partial x}\right)\bigg|_{x=x_a} + Q_6\left(-\frac{\partial\psi_i^{(2)}}{\partial x}\right)\bigg|_{x=x_b}
\end{aligned}
\tag{12.4.27}
$$

It is important to note that nonlinear quantities in the stiffness coefficients of Eq. (12.4.26) and throughout the remainder of this section are functions of current time t (as opposed to s), unless explicitly stated otherwise.

12.4.4.2 The Timoshenko beam finite element

To construct the finite element model for the TBT, we approximate the dependent variables using the following independent finite element interpolations:

$$
\begin{aligned}
u(x,t) &= \sum_{j=1}^{p_1} \Delta_j^1(t)\psi_j^{(1)}(x) \\
w(x,t) &= \sum_{j=1}^{p_2} \Delta_j^2(t)\psi_j^{(2)}(x) \\
\phi_x(x,t) &= \sum_{j=1}^{p_3} \Delta_j^3(t)\psi_j^{(3)}(x)
\end{aligned}
\tag{12.4.28}
$$

where $\psi_j^{(\alpha)} \in H^1(\Omega^e)$ $(\alpha = 1,2,3)$ are Lagrange interpolation functions of degree (p_1-1), (p_2-1), and (p_3-1), respectively. The Lagrange interpolation functions are defined as [2]

$$
\psi_j^{(\alpha)}(\xi) = \prod\nolimits_{k=1,k\neq j}^{p_\alpha} \frac{\xi - \xi_k}{\xi_j - \xi_k}
\tag{12.4.29}
$$

where ξ_k is the value of ξ at the kth node of a typical finite element. The quantities $\Delta_j^\alpha(t)$ are once again the generalized displacements at the nodes.

Substituting Eq. (12.4.28) into Eqs. (12.4.13)–(12.4.15), we obtain the semi-discrete finite element equations (i.e. ordinary differential equations in time) for the Timoshenko beam theory. The resulting matrices can be defined by the following expressions [compare with Eq. (5.3.26)]:

$$
\begin{aligned}
K_{ij}^{11} &= \int_{x_a}^{x_b} E(0)A\frac{d\psi_i^{(1)}}{dx}\frac{d\psi_j^{(1)}}{dx}dx \\
K_{ij}^{12} &= \frac{1}{2}K_{ji}^{21} = \frac{1}{2}\int_{x_a}^{x_b}\Big(E(0)A\,\frac{\partial w}{\partial x}\Big)\frac{d\psi_i^{(1)}}{dx}\frac{d\psi_j^{(2)}}{dx}dx
\end{aligned}
$$

$$
\begin{aligned}
K_{ij}^{13} &= K_{ji}^{31} = \tilde{K}_{ij}^{13} = \tilde{K}_{ji}^{31} = 0\\
K_{ij}^{22} &= \int_{x_a}^{x_b} A\Big[\frac{1}{2}E(0)\Big(\frac{\partial w}{\partial x}\Big)^2 + K_s G(0)\Big]\frac{d\psi_i^{(2)}}{dx}\frac{d\psi_j^{(2)}}{dx}dx\\
K_{ij}^{23} &= K_{ji}^{32} = \int_{x_a}^{x_b} K_s G(0) A\,\frac{d\psi_i^{(2)}}{dx}\psi_j^{(3)}dx\\
K_{ij}^{33} &= \int_{x_a}^{x_b}\Big(E(0)I\,\frac{d\psi_i^{(3)}}{dx}\frac{d\psi_j^{(3)}}{dx} + K_s G(0) A\,\psi_i^{(3)}\psi_j^{(3)}\Big)dx\\
\tilde{K}_{ij}^{11} &= \int_{x_a}^{x_b}\dot{E}(t-s)A\,\frac{d\psi_i^{(1)}}{dx}\frac{d\psi_j^{(1)}}{dx}dx\\
\tilde{K}_{ij}^{12} &= \frac{1}{2}\int_{x_a}^{x_b}\Big(\dot{E}(t-s)A\,\frac{\partial w(x,s)}{\partial x}\Big)\frac{d\psi_i^{(1)}}{dx}\frac{d\psi_j^{(2)}}{dx}dx\\
\tilde{K}_{ij}^{21} &= \int_{x_a}^{x_b}\Big(\dot{E}(t-s)A\,\frac{\partial w\,(x,s)}{\partial x}\Big)\frac{d\psi_i^{(2)}}{dx}\frac{d\psi_j^{(1)}}{dx}dx\\
\tilde{K}_{ij}^{22} &= \int_{x_a}^{x_b} A\Big(\frac{1}{2}\dot{E}(t-s)\frac{\partial w}{\partial x}\frac{\partial w(x,s)}{\partial x} + K_s\dot{G}(t-s)\Big)\frac{d\psi_i^{(2)}}{dx}\frac{d\psi_j^{(2)}}{dx}dx\\
\tilde{K}_{ij}^{23} &= \tilde{K}_{ji}^{32} = \int_{x_a}^{x_b} K_s\dot{G}(t-s)A\,\frac{d\psi_i^{(2)}}{dx}\psi_j^{(3)}dx\\
\tilde{K}_{ij}^{33} &= \int_{x_a}^{x_b}\Big(\dot{E}(t-s)I\,\frac{d\psi_i^{(3)}}{dx}\frac{d\psi_j^{(3)}}{dx} + K_s\dot{G}(t-s)A\,\psi_i^{(3)}\psi_j^{(3)}\Big)dx
\end{aligned}
\tag{12.4.30}
$$

and

$$
\begin{aligned}
F_i^1 &= \int_{x_a}^{x_b}\psi_i^{(1)} f dx + Q_1\psi_i^{(1)}(x_a) + Q_4\psi_i^{(1)}(x_b)\\
F_i^2 &= \int_{x_a}^{x_b}\psi_i^{(2)} q dx + Q_2\psi_i^{(2)}(x_a) + Q_5\psi_i^{(2)}(x_b)\\
F_i^3 &= Q_3\psi_i^{(3)}(x_a) + Q_6\psi_i^{(3)}(x_b)
\end{aligned}
\tag{12.4.31}
$$

12.4.5 Fully Discretized Finite Element Models

12.4.5.1 Time discretization using recurrence formulae

The fully discretized finite element equations are obtained by partitioning the time interval $[0,T]\subset\mathbb{R}$ of interest in the analysis into a set of N non-overlapping subintervals such that

$$
[0,T] = \bigcup_{k=1}^{N}[t_k, t_{k+1}] \tag{12.4.32}
$$

The solution is obtained by solving an initial value problem within each subregion $\left[t_k, t_{k+1}\right]$, where the solution is known at $t = t_k$. The convolution integral present in the semi-discrete finite element equations is approximated using the trapezoidal rule within each time interval. A direct temporal integration, however, is computationally unattractive as it requires the need to store the entire deformation history. When N is large, the computational time expended at a given time step can become dominated by the evaluation of the convolution integral.

In the present analysis we develop a recurrence formula for evaluating the convolution terms that circumvents the need to explicitly store and use the entire deformation history. The present formulation requires only the storage of the generalized displacements and a set of internal variables evaluated at the Gauss points, both from the previous time step only. In presenting the general ideas we note that the convolution integral appearing in Eq. (12.4.19) can be expressed as

$$\int_0^{t_N} \left[\tilde{K}\right]\left\{\Delta\left(s\right)\right\} ds = \sum_{k=1}^{N-1} \int_{t_k}^{t_{k+1}} \left[\tilde{K}\right]\left\{\Delta\left(s\right)\right\} ds \tag{12.4.33}$$

The recurrence formulation relies on the following multiplicative decomposition of the relaxation moduli [324]

$$\begin{aligned} \dot{E}\left(t_{k+1} - s\right) &= \sum_{l=1}^{n} e^{-\frac{\Delta t_k}{\tau_l^E}} \dot{E}_l\left(t_k - s\right) \\ \dot{G}\left(t_{k+1} - s\right) &= \sum_{l=1}^{n} e^{-\frac{\Delta t_k}{\tau_l^G}} \dot{G}_l\left(t_k - s\right) \end{aligned} \tag{12.4.34}$$

where $\Delta t_k = t_{k+1} - t_k$. The above equations hold since the relaxation moduli are expressed in terms of Prony series. Equation (12.4.33) can be expressed in index notation at an arbitrary time step $t = t_s$ as

$$X_i\left(t_s\right) = \sum_{k=1}^{s-1} \int_{t_k}^{t_{k+1}} \tilde{K}_{ij} \Delta_j\left(s\right) ds \cong \sum_{l=1}^{n} \sum_{m=1}^{NGP} \alpha_m \bar{X}_i^{lm}\left(t_s\right) \tag{12.4.35}$$

where α_m are parameters and Einstein's summation convention is used. In the above expression we have approximated each temporal integral using the trapezoidal rule. As noted previously, Gauss quadrature is employed in evaluation of $\tilde{K}_{ij}$, resulting in the summation over m (where NGP is the number of Gauss points). In practice the above approximation is applied in the evaluation of each temporal integral of the individual terms comprising each component $\tilde{K}_{ij}^{\gamma\beta} \Delta_j^{\beta}(s)$. When applied to a specific term, the quantity $\bar{X}_i^{lm}\left(t_s\right)$ assumes the following possible forms:

$$\bar{X}_i^{lm}(t_s) = e^{-\frac{\Delta t_{s-1}}{\tau_l^E}} \bar{X}_i^{lm}(t_{s-1}) - 2\Gamma_l^E \left(e^{-\frac{\Delta t_{s-1}}{\tau_l^E}} g_i^m(t_{s-1}) + g_i^m(t_s) \right) \tag{12.4.36}$$

$$\bar{X}_i^{lm}(t_s) = e^{-\frac{\Delta t_{s-1}}{\tau_l^G}} \bar{X}_i^{lm}(t_{s-1}) - 2\Gamma_l^G \left(e^{-\frac{\Delta t_{s-1}}{\tau_l^G}} g_i^m(t_{s-1}) + g_i^m(t_s) \right) \tag{12.4.37}$$

where

$$\Gamma_l^E = \frac{\Delta t_{s-1}}{4} \frac{E_l}{\tau_l^E}, \quad \Gamma_l^G = \frac{\Delta t_{s-1}}{4} \frac{G_l}{\tau_l^G} \tag{12.4.38}$$

and Eq. (12.4.36) is used to approximate the integral of $\tilde{K}_{ij}^{\gamma\beta} \Delta_j^\beta(s)$ involving viscoelastic relaxation quantities. Likewise Eq. (12.4.37) is employed for quantities involving shear terms. The specific forms of α_m and $g_i^m(t_s)$ vary for each component. The above equations represent recurrence formulae in terms of the internal variables $\bar{X}_i^{lm}(t_s)$ that bypass the need to store solution data at every time step in the evaluation of Eq. (12.4.35). The present formulation therefore requires the retention of $\{\Delta(t_s)\}$ and $\bar{X}_i^{lm}(t_{s-1})$ only. We note that $\bar{X}_i^{lm}(t_1) = 0$.

Using Eqs. (12.4.35)–(12.4.37) we obtain the following set of finite element equations for the generalized displacements at the current time step

$$[\bar{K}]_s \{\Delta\}_s = \{F\}_s - \{\tilde{Q}\}_s \tag{12.4.39}$$

where we have introduced the notation $\{\Delta\}_s = \{\Delta(t_s)\}$. The specific forms of $[\bar{K}]_s$ and $\{\tilde{Q}\}_s$ for each beam theory are presented in the next section.

Next, we present formulae for determining the components of the fully discretized EBT and TBT finite element models. Formulae for determining the tangent stiffness matrices arising from the Newton linearization of the finite element equations are also provided.

12.4.5.2 The Euler–Bernoulli beam finite element

The additional matrices introduced in the fully discretized form of the EBT finite element equations can be determined from the following formulae:

$$\bar{K}_{ij}^{11} = \int_{x_a}^{x_b} \left(E(0) + \frac{\Delta t_{s-1}}{2} \dot{E}(0) \right) A \frac{d\psi_i^{(1)}}{dx} \frac{d\psi_j^{(1)}}{dx} dx$$

$$\bar{K}_{ij}^{12} = \frac{1}{2} \int_{x_a}^{x_b} \left(E(0) + \frac{\Delta t_{s-1}}{2} \dot{E}(0) \right) \left(A \frac{\partial w}{\partial x} \right) \frac{d\psi_i^{(1)}}{dx} \frac{d\psi_j^{(2)}}{dx} dx$$

$$\bar{K}_{ij}^{21} = \int_{x_a}^{x_b} \left(E\left(0\right) + \frac{\Delta t_{s-1}}{2}\dot{E}\left(0\right)\right)\left(A\frac{\partial w}{\partial x}\right)\frac{d\psi_i^{(2)}}{dx}\frac{d\psi_j^{(1)}}{dx}dx \qquad (12.4.40)$$

$$\bar{K}_{ij}^{22} = \int_{x_a}^{x_b} \left(E\left(0\right) + \frac{\Delta t_{s-1}}{2}\dot{E}\left(0\right)\right) I\frac{d^2\psi_i^{(2)}}{dx^2}\frac{d^2\psi_j^{(2)}}{dx^2}dx + \frac{1}{2}\int_{x_a}^{x_b} \left(E\left(0\right) + \frac{\Delta t_{s-1}}{2}\dot{E}\left(0\right)\right) A\left(\frac{\partial w}{\partial x}\right)^2\frac{d\psi_i^{(2)}}{dx}\frac{d\psi_j^{(2)}}{dx}dx$$

The components of the viscoelastic force vector $\{\tilde{Q}\}_s$ can be expressed as

$$\{\tilde{Q}^1\}_s = \{{}^1\bar{Q}^1\} + \{{}^2\bar{Q}^1\}, \quad \{\tilde{Q}^2\}_s = \{{}^1\bar{Q}^2\} + \{{}^2\bar{Q}^2\} + \{{}^3\bar{Q}^2\} \qquad (12.4.41)$$

where

$${}^1\bar{Q}_i^1 = \dot{E}\left(\Delta t_{s-1}\right)\frac{\Delta t_{s-1}}{2}\left[\int_{x_a}^{x_b} A\frac{d\psi_i^{(1)}}{dx}\frac{d\psi_j^{(1)}}{dx}dx\right]\Delta_j^1\left(t_{s-1}\right) + \sum_{l=1}^{n}\sum_{m=1}^{NGP} e^{-\frac{\Delta t_{s-1}}{\tau_l^E}}\, {}^1\bar{X}_i^{lm}\left(t_{s-1}\right) \qquad (12.4.42)$$

$${}^2\bar{Q}_i^1 = \frac{\Delta t_{s-1}}{4}\dot{E}\left(\Delta t_{s-1}\right)\left[\int_{x_a}^{x_b} A\frac{\partial w\left(x, t_{s-1}\right)}{\partial x}\frac{d\psi_i^{(1)}}{dx}\frac{d\psi_j^{(2)}}{dx}dx\right]\Delta_j^2\left(t_{s-1}\right) + \sum_{l=1}^{n}\sum_{m=1}^{NGP} e^{-\frac{\Delta t_{s-1}}{\tau_l^E}}\, {}^2\bar{X}_i^{lm}\left(t_{s-1}\right) \qquad (12.4.43)$$

$${}^1\bar{Q}_i^2 = \dot{E}\left(\Delta t_{s-1}\right)\frac{\Delta t_{s-1}}{2}\left[\int_{x_a}^{x_b} A\frac{\partial w\left(x, t_{s-1}\right)}{\partial x}\frac{d\psi_i^{(2)}}{dx}\frac{d\psi_j^{(1)}}{dx}dx\right]\Delta_j^1\left(t_{s-1}\right) + \sum_{l=1}^{n}\sum_{m=1}^{NGP} e^{-\frac{\Delta t_{s-1}}{\tau_l^E}}\frac{\partial w\left(x_m, t_s\right)}{\partial x}\, {}^3\bar{X}_i^{lm}\left(t_{s-1}\right) \qquad (12.4.44)$$

$${}^2\bar{Q}_i^2 = \dot{E}\left(\Delta t_{s-1}\right)\frac{\Delta t_{s-1}}{2}\left[\int_{x_a}^{x_b} I\frac{d^2\psi_i^{(2)}}{dx^2}\frac{d^2\psi_j^{(2)}}{dx^2}dx\right]\Delta_j^2\left(t_{s-1}\right) + \sum_{l=1}^{n}\sum_{m=1}^{NGP} e^{-\frac{\Delta t_{s-1}}{\tau_l^E}}\, {}^4\bar{X}_i^{lm}\left(t_{s-1}\right) \qquad (12.4.45)$$

$${}^3\bar{Q}_i^2 = \dot{E}\left(\Delta t_{s-1}\right)\frac{\Delta t_{s-1}}{4}\left[\int_{x_a}^{x_b} A\frac{\partial w\left(x, t_{s-1}\right)}{\partial x}\frac{\partial w\left(x, t_{s-1}\right)}{\partial x}\frac{d\psi_i^{(2)}}{dx}\frac{d\psi_j^{(2)}}{dx}dx\right]\Delta_j^2\left(t_{s-1}\right) + \sum_{l=1}^{n}\sum_{m=1}^{NGP} e^{-\frac{\Delta t_{s-1}}{\tau_l^E}}\frac{\partial w\left(x_m, t_s\right)}{\partial x}\, {}^5\bar{X}_i^{lm}\left(t_{s-1}\right) \qquad (12.4.46)$$

The history terms ${}^{j}\bar{X}_{i}^{lm}\left(t_s\right)$ introduced in Eqs. (12.4.42)–(12.4.46) can be expressed as

$$
\begin{aligned}
{}^{1}\bar{X}_{i}^{lm}\left(t_s\right) = & -2\Gamma_l^E A \frac{d\psi_i^{(1)}\left(x_m\right)}{dx}\frac{d\psi_j^{(1)}\left(x_m\right)}{dx}\left(e^{-\frac{\Delta t_{s-1}}{\tau_l^E}}\Delta_j^1\left(t_{s-1}\right)+\Delta_j^1\left(t_s\right)\right)W_m \\
& +e^{-\frac{\Delta t_{s-1}}{\tau_l^E}}\,{}^{1}\bar{X}_{i}^{lm}\left(t_{s-1}\right)
\end{aligned} \tag{12.4.47}
$$

$$
\begin{aligned}
{}^{2}\bar{X}_{i}^{lm}\left(t_s\right) = & -\Gamma_l^E A \frac{d\psi_i^{(1)}\left(x_m\right)}{dx}\frac{d\psi_j^{(2)}\left(x_m\right)}{dx}\left(\frac{\partial w\left(x_m,t_{s-1}\right)}{\partial x}e^{-\frac{\Delta t_{s-1}}{\tau_l^E}}\Delta_j^2\left(t_{s-1}\right)\right. \\
& \left.+\frac{\partial w\left(x_m,t_s\right)}{\partial x}\Delta_j^2\left(t_s\right)\right)W_m+e^{-\frac{\Delta t_{s-1}}{\tau_l^E}}\,{}^{2}\bar{X}_{i}^{lm}\left(t_{s-1}\right)
\end{aligned} \tag{12.4.48}
$$

$$
\begin{aligned}
{}^{3}\bar{X}_{i}^{lm}\left(t_s\right) = & -2\Gamma_l^E A \frac{d\psi_i^{(2)}\left(x_m\right)}{dx}\frac{d\psi_j^{(1)}\left(x_m\right)}{dx}\left(e^{-\frac{\Delta t_{s-1}}{\tau_l^E}}\Delta_j^1\left(t_{s-1}\right)+\Delta_j^1\left(t_s\right)\right)W_m \\
& +e^{-\frac{\Delta t_{s-1}}{\tau_l^E}}\,{}^{3}\bar{X}_{i}^{lm}\left(t_{s-1}\right)
\end{aligned} \tag{12.4.49}
$$

$$
\begin{aligned}
{}^{4}\bar{X}_{i}^{lm}\left(t_s\right) = & -2\Gamma_l^E I \frac{d^2\psi_i^{(2)}\left(x_m\right)}{dx^2}\frac{d^2\psi_j^{(2)}\left(x_m\right)}{dx^2}\left(e^{-\frac{\Delta t_{s-1}}{\tau_l^E}}\Delta_j^2\left(t_{s-1}\right)+\Delta_j^2\left(t_s\right)\right)W_m \\
& +e^{-\frac{\Delta t_{s-1}}{\tau_l^E}}\,{}^{4}\bar{X}_{i}^{lm}\left(t_{s-1}\right)
\end{aligned} \tag{12.4.50}
$$

$$
\begin{aligned}
{}^{5}\bar{X}_{i}^{lm}\left(t_s\right) = & -\Gamma_l^E A \frac{d\psi_i^{(2)}\left(x_m\right)}{dx}\frac{d\psi_j^{(2)}\left(x_m\right)}{dx}\left(\frac{\partial w\left(x_m,t_{s-1}\right)}{\partial x}e^{-\frac{\Delta t_{s-1}}{\tau_l^E}}\Delta_j^2\left(t_{s-1}\right)\right. \\
& \left.+\frac{\partial w\left(x_m,t_s\right)}{\partial x}\Delta_j^2\left(t_s\right)\right)W_m+e^{-\frac{\Delta t_{s-1}}{\tau_l^E}}\,{}^{5}\bar{X}_{i}^{lm}\left(t_{s-1}\right)
\end{aligned} \tag{12.4.51}
$$

where W_m are the Gauss weights. In the evaluation of ${}^{k}\bar{X}_{i}^{lm}$, it is necessary to express the interpolation functions $\psi_i^{(\alpha)}$ and nonlinear quantities in terms of the natural coordinate ξ. Einstein's summation convention has been used extensively on the j indices in the above formulae.

12.4.5.3 The Timoshenko beam finite element

For the Timoshenko beam theory, the additional matrices introduced in the fully discrete form of the finite element equations can be expressed as

$$
\begin{aligned}
\bar{K}_{ij}^{11} &= \int_{x_a}^{x_b}\left(E\left(0\right)+\frac{\Delta t_{s-1}}{2}\dot{E}\left(0\right)\right)A\frac{d\psi_i^{(1)}}{dx}\frac{d\psi_j^{(1)}}{dx}dx \\
\bar{K}_{ij}^{12} &= \frac{1}{2}\bar{K}_{ji}^{21}=\frac{1}{2}\int_{x_a}^{x_b}\left(E\left(0\right)+\frac{\Delta t_{s-1}}{2}\dot{E}\left(0\right)\right)A\frac{\partial w}{\partial x}\frac{d\psi_i^{(1)}}{dx}\frac{d\psi_j^{(2)}}{dx}dx
\end{aligned}
$$

$$\bar{K}_{ij}^{13} = \bar{K}_{ji}^{31} = 0$$

$$\begin{aligned}\bar{K}_{ij}^{22} &= \int_{x_a}^{x_b} \left[\frac{1}{2}\left(E(0) + \frac{\Delta t_{s-1}}{2}\dot{E}(0)\right)\left(\frac{\partial w}{\partial x}\right)^2 \right.\\ &\left. \quad + K_s\left(G(0) + \frac{\Delta t_{s-1}}{2}\dot{G}(0)\right)\right] A\frac{d\psi_i^{(2)}}{dx}\frac{d\psi_j^{(2)}}{dx}dx \qquad (12.4.52)\\ \bar{K}_{ij}^{23} &= \bar{K}_{ji}^{32} = \int_{x_a}^{x_b}\left(G(0) + \frac{\Delta t_{s-1}}{2}\dot{G}(0)\right)K_s A\frac{d\psi_i^{(2)}}{dx}\psi_j^{(3)}dx\\ \bar{K}_{ij}^{33} &= \int_{x_a}^{x_b}\left[\left(E(0) + \frac{\Delta t_{s-1}}{2}\dot{E}(0)\right) I\frac{d\psi_i^{(3)}}{dx}\frac{d\psi_j^{(3)}}{dx}\right.\\ &\left. \quad + \left(G(0) + \frac{\Delta t_{s-1}}{2}\dot{G}(0)\right)K_s A\psi_i^{(3)}\psi_j^{(3)}\right]dx\end{aligned}$$

The components of the viscoelastic force vector $\{\tilde{Q}\}_s$ can be expressed as

$$\begin{aligned}&\{\tilde{Q}^1\}_s = \{{}^1\bar{Q}^1\}+\{{}^2\bar{Q}^1\}, \quad \{\tilde{Q}^3\}_s = \{{}^1\bar{Q}^3\}+\{{}^2\bar{Q}^3\}+\{{}^3\bar{Q}^3\}\\ &\{\tilde{Q}^2\}_s = \{{}^1\bar{Q}^2\}+\{{}^2\bar{Q}^2\}+\{{}^3\bar{Q}^2\}+\{{}^4\bar{Q}^2\}\end{aligned} \qquad (12.4.53)$$

where

$$\begin{aligned}{}^1\bar{Q}_i^1 &= \dot{E}(\Delta t_{s-1})\frac{\Delta t_{s-1}}{2}\left[\int_{x_a}^{x_b} A\frac{d\psi_i^{(1)}}{dx}\frac{d\psi_j^{(1)}}{dx}dx\right]\Delta_j^1(t_{s-1})\\ &\quad + \sum_{l=1}^{n}\sum_{m=1}^{NGP} e^{-\frac{\Delta t_{s-1}}{\tau_l^E}}\,{}^1\bar{X}_i^{lm}(t_{s-1}) \qquad (12.4.54)\end{aligned}$$

$$\begin{aligned}{}^2\bar{Q}_i^1 &= \dot{E}(\Delta t_{s-1})\frac{\Delta t_{s-1}}{4}\left[\int_{x_a}^{x_b} A\frac{\partial w(x,t_{s-1})}{\partial x}\frac{d\psi_i^{(1)}}{dx}\frac{d\psi_j^{(2)}}{dx}dx\right]\Delta_j^2(t_{s-1})\\ &\quad + \sum_{l=1}^{n}\sum_{m=1}^{NGP} e^{-\frac{\Delta t_{s-1}}{\tau_l^E}}\,{}^2\bar{X}_i^{lm}(t_{s-1}) \qquad (12.4.55)\end{aligned}$$

$$\begin{aligned}{}^1\bar{Q}_i^2 &= \dot{E}(\Delta t_{s-1})\frac{\Delta t_{s-1}}{2}\left[\int_{x_a}^{x_b} A\frac{\partial w(x,t_s)}{\partial x}\frac{d\psi_i^{(2)}}{dx}\frac{d\psi_j^{(1)}}{dx}dx\right]\Delta_j^1(t_{s-1})\\ &\quad + \sum_{l=1}^{n}\sum_{m=1}^{NGP} e^{-\frac{\Delta t_{s-1}}{\tau_l^E}}\frac{\partial w(x_m,t_s)}{\partial x}\,{}^3\bar{X}_i^{lm}(t_{s-1}) \qquad (12.4.56)\end{aligned}$$

$$\begin{aligned}{}^2\bar{Q}_i^2 &= \dot{E}(\Delta t_{s-1})\frac{\Delta t_{s-1}}{4}\left[\int_{x_a}^{x_b} A\frac{\partial w(x,t_s)}{\partial x}\frac{\partial w(x,t_{s-1})}{\partial x}\frac{d\psi_i^{(2)}}{dx}\frac{d\psi_j^{(2)}}{dx}dx\right]\Delta_j^2(t_{s-1})\\ &\quad + \sum_{l=1}^{n}\sum_{m=1}^{NGP} e^{-\frac{\Delta t_{s-1}}{\tau_l^E}}\frac{\partial w(x_m,t_s)}{\partial x}\,{}^4\bar{X}_i^{lm}(t_{s-1}) \qquad (12.4.57)\end{aligned}$$

$$
\begin{aligned}
{}^{3}\bar{Q}_i^2 &= K_s\dot{G}\left(\Delta t_{s-1}\right)\frac{\Delta t_{s-1}}{2}\left[\int_{x_a}^{x_b} A\frac{d\psi_i^{(2)}}{dx}\frac{d\psi_j^{(2)}}{dx}dx\right]\Delta_j^2\left(t_{s-1}\right)\\
&\quad+\sum_{l=1}^{n}\sum_{m=1}^{NGP} e^{-\frac{\Delta t_{s-1}}{\tau_l^G}}\,{}^{5}\bar{X}_i^{lm}\left(t_{s-1}\right) \qquad (12.4.58)\\
{}^{4}\bar{Q}_i^2 &= K_s\dot{G}\left(\Delta t_{s-1}\right)\frac{\Delta t_{s-1}}{2}\left[\int_{x_a}^{x_b} A\frac{d\psi_i^{(2)}}{dx}\psi_j^{(3)}dx\right]\Delta_j^3\left(t_{s-1}\right)\\
&\quad+\sum_{l=1}^{n}\sum_{m=1}^{NGP} e^{-\frac{\Delta t_{s-1}}{\tau_l^G}}\,{}^{6}\bar{X}_i^{lm}\left(t_{s-1}\right) \qquad (12.4.59)\\
{}^{1}\bar{Q}_i^3 &= K_s\dot{G}\left(\Delta t_{s-1}\right)\frac{\Delta t_{s-1}}{2}\left[\int_{x_a}^{x_b} A\psi_i^{(3)}\frac{d\psi_j^{(2)}}{dx}dx\right]\Delta_j^2\left(t_{s-1}\right)\\
&\quad+\sum_{l=1}^{n}\sum_{m=1}^{NGP} e^{-\frac{\Delta t_{s-1}}{\tau_l^G}}\,{}^{7}\bar{X}_i^{lm}\left(t_{s-1}\right) \qquad (12.4.60)\\
{}^{2}\bar{Q}_i^3 &= \dot{E}\left(\Delta t_{s-1}\right)\frac{\Delta t_{s-1}}{2}\left[\int_{x_a}^{x_b} I\frac{d\psi_i^{(3)}}{dx}\frac{d\psi_j^{(3)}}{dx}dx\right]\Delta_j^3\left(t_{s-1}\right)\\
&\quad+\sum_{l=1}^{n}\sum_{m=1}^{NGP} e^{-\frac{\Delta t_{s-1}}{\tau_l^E}}\,{}^{8}\bar{X}_i^{lm}\left(t_{s-1}\right) \qquad (12.4.61)\\
{}^{3}\bar{Q}_i^3 &= K_s\dot{G}\left(\Delta t_{s-1}\right)\frac{\Delta t_{s-1}}{2}\left[\int_{x_a}^{x_b} A\psi_i^{(3)}\psi_j^{(3)}dx\right]\Delta_j^3\left(t_{s-1}\right)\\
&\quad+\sum_{l=1}^{n}\sum_{m=1}^{NGP} e^{-\frac{\Delta t_{s-1}}{\tau_l^G}}\,{}^{9}\bar{X}_i^{lm}\left(t_{s-1}\right) \qquad (12.4.62)
\end{aligned}
$$

The history terms ${}^{j}\bar{X}_i^{lm}\left(t_s\right)$ introduced in Eqs. (12.4.54)–(12.4.62) can be expressed as

$$
\begin{aligned}
{}^{1}\bar{X}_i^{lm}\left(t_s\right) &= -2\Gamma_l^E A\frac{d\psi_i^{(1)}\left(x_m\right)}{dx}\frac{d\psi_j^{(1)}\left(x_m\right)}{dx}\Big[e^{-\frac{\Delta t_{s-1}}{\tau_l^E}}\Delta_j^1\left(t_{s-1}\right)+\Delta_j^1\left(t_s\right)\Big]W_m\\
&\quad+e^{-\frac{\Delta t_{s-1}}{\tau_l^E}}\,{}^{1}\bar{X}_i^{lm}\left(t_{s-1}\right) \qquad (12.4.63)\\
{}^{2}\bar{X}_i^{lm}\left(t_s\right) &= -2\Gamma_l^E A\Big[\frac{1}{2}e^{-\frac{\Delta t_{s-1}}{\tau_l^E}}\frac{\partial w\left(x_m,t_{s-1}\right)}{\partial x}\frac{d\psi_i^{(1)}\left(x_m\right)}{dx}\frac{d\psi_j^{(2)}\left(x_m\right)}{dx}\Delta_j^2\left(t_{s-1}\right)\\
&\quad+\frac{1}{2}\frac{\partial w\left(x_m,t_s\right)}{\partial x}\frac{d\psi_i^{(1)}\left(x_m\right)}{dx}\frac{d\psi_j^{(2)}\left(x_m\right)}{dx}\Delta_j^2\left(t_s\right)\Big]W_m\\
&\quad+e^{-\frac{\Delta t_{s-1}}{\tau_l^E}}\,{}^{2}\bar{X}_i^{lm}\left(t_{s-1}\right) \qquad (12.4.64)
\end{aligned}
$$

$$
\begin{aligned}
{}^{3}\bar{X}_i^{lm}(t_s) = & -2\Gamma_l^E A \frac{d\psi_i^{(2)}(x_m)}{dx}\frac{d\psi_j^{(1)}(x_m)}{dx}\Big[e^{-\frac{\Delta t_{s-1}}{\tau_l^E}}\Delta_j^1(t_{s-1})+\Delta_j^1(t_s)\Big]W_m \\
& + e^{-\frac{\Delta t_{s-1}}{\tau_l^E}}\,{}^{3}\bar{X}_i^{lm}(t_{s-1})
\end{aligned} \tag{12.4.65}
$$

$$
\begin{aligned}
{}^{4}\bar{X}_i^{lm}(t_s) = & -\Gamma_l^E A\Big[e^{-\frac{\Delta t_{s-1}}{\tau_l^E}}\frac{\partial w(x_m,t_{s-1})}{\partial x}\frac{d\psi_i^{(2)}(x_m)}{dx}\frac{d\psi_j^{(2)}(x_m)}{dx}\Delta_j^2(t_{s-1}) \\
& + \frac{\partial w(x_m,t_s)}{\partial x}\frac{d\psi_i^{(2)}(x_m)}{dx}\frac{d\psi_j^{(2)}(x_m)}{dx}\Delta_j^2(t_s)\Big]W_m \\
& + e^{-\frac{\Delta t_{s-1}}{\tau_l^E}}\,{}^{4}\bar{X}_i^{lm}(t_{s-1})
\end{aligned} \tag{12.4.66}
$$

$$
\begin{aligned}
{}^{5}\bar{X}_i^{lm}(t_s) = & -\Gamma_l^G K_s A \frac{d\psi_i^{(2)}(x_m)}{dx}\frac{d\psi_j^{(2)}(x_m)}{dx}\Big(e^{-\frac{\Delta t_{s-1}}{\tau_l^G}}\Delta_j^2(t_{s-1})+\Delta_j^2(t_s)\Big)W_m \\
& + e^{-\frac{\Delta t_{s-1}}{\tau_l^G}}\,{}^{5}\bar{X}_i^{lm}(t_{s-1})
\end{aligned} \tag{12.4.67}
$$

$$
\begin{aligned}
{}^{6}\bar{X}_i^{lm}(t_s) = & -\Gamma_l^G K_s A \frac{d\psi_i^{(2)}(x_m)}{dx}\psi_j^{(3)}(x_m)\Big[e^{-\frac{\Delta t_{s-1}}{\tau_l^G}}\Delta_j^3(t_{s-1})+\Delta_j^3(t_s)\Big]W_m \\
& + e^{-\frac{\Delta t_{s-1}}{\tau_l^G}}\,{}^{6}\bar{X}_i^{lm}(t_{s-1})
\end{aligned} \tag{12.4.68}
$$

$$
\begin{aligned}
{}^{7}\bar{X}_i^{lm}(t_s) = & -\Gamma_l^G K_s A \psi_i^{(3)}(x_m)\frac{d\psi_j^{(2)}(x_m)}{dx}\Big[e^{-\frac{\Delta t_{s-1}}{\tau_l^G}}\Delta_j^2(t_{s-1})+\Delta_j^2(t_s)\Big]W_m \\
& + e^{-\frac{\Delta t_{s-1}}{\tau_l^G}}\,{}^{7}\bar{X}_i^{lm}(t_{s-1})
\end{aligned} \tag{12.4.69}
$$

$$
\begin{aligned}
{}^{8}\bar{X}_i^{lm}(t_s) = & -2\Gamma_l^E I \frac{d\psi_i^{(3)}(x_m)}{dx}\frac{d\psi_j^{(3)}(x_m)}{dx}\Big(e^{-\frac{\Delta t_{s-1}}{\tau_l^E}}\Delta_j^3(t_{s-1})+\Delta_j^3(t_s)\Big)W_m \\
& + e^{-\frac{\Delta t_{s-1}}{\tau_l^E}}\,{}^{8}\bar{X}_i^{lm}(t_{s-1})
\end{aligned} \tag{12.4.70}
$$

$$
\begin{aligned}
{}^{9}\bar{X}_i^{lm}(t_s) = & -\Gamma_l^G K_s A \psi_i^{(3)}(x_m)\psi_j^{(3)}(x_m)\Big(e^{-\frac{\Delta t_{s-1}}{\tau_l^G}}\Delta_j^3(t_{s-1})+\Delta_j^3(t_s)\Big)W_m \\
& + e^{-\frac{\Delta t_{s-1}}{\tau_l^G}}\,{}^{9}\bar{X}_i^{lm}(t_{s-1})
\end{aligned} \tag{12.4.71}
$$

12.4.5.4 Solution of nonlinear equations using Newton's method

The fully discretized finite element equations are nonlinear due to the inclusion of the *von Kármán* strains in the formulation. For our analysis we solve the equations iteratively using the Newton linearization procedure. The resulting linearized equations are of the form

$$
\{\Delta\}_s^{(r)} = \{\Delta\}_s^{(r-1)} - [T]_s^{-1}\Big([\bar{K}]_s^{(r-1)}\{\Delta\}_s^{(r-1)} - \{F\}_s^{(r-1)} + \{\tilde{Q}\}_s^{(r-1)}\Big) \tag{12.4.72}
$$

where $\{\Delta\}_s^{(r)}$ represents the solution at the rth iteration and time $t = t_s$. The tangent stiffness matrix $[T]_s$ in Eq. (12.4.72) is defined using Einstein's summation notation as

$$T_{ij}^{\alpha\beta} = \frac{\partial}{\partial \Delta_j^\beta} \left(\sum_{\gamma=1}^{k} \sum_{p=1}^{n(\gamma)} \bar{K}_{ip}^{\alpha\gamma} \Delta_p^\gamma - \tilde{Q}_i^\alpha \right) \tag{12.4.73}$$

where $k = 2$ for the EBT and $k = 3$ for the TBT. All quantities in Eq. (12.4.73) comprising the tangent stiffness matrix are formulated using the solution from the $(r-1)$th iteration. It is important to note that all partial derivatives are taken with respect to the solution at the current time step.

Applying Newton's method to the Euler–Bernoulli beam equations results in the following component representation of the tangent stiffness matrix

$$T_{ij}^{11} = \bar{K}_{ij}^{11}, \qquad T_{ij}^{12} = 2\bar{K}_{ij}^{12}, \qquad T_{ij}^{21} = \bar{K}_{ij}^{21}$$

$$\begin{aligned} T_{ij}^{22} = \bar{K}_{ij}^{22} &+ \int_{x_a}^{x_b} A \left\{ \left(E(0) + \frac{\Delta t_{s-1}}{2} \dot{E}(0) \right) \left[\frac{\partial u}{\partial x} + \left(\frac{\partial w}{\partial x} \right)^2 \right] \right. \\ &\left. + \frac{\Delta t_{s-1}}{2} \dot{E}(\Delta t_{s-1}) \left[\frac{\partial u(x, t_{s-1})}{\partial x} + \frac{1}{2} \left(\frac{\partial w(x, t_{s-1})}{\partial x} \right)^2 \right] \right\} \frac{d\psi_i^{(2)}}{dx} \frac{d\psi_j^{(2)}}{dx} dx \\ &+ \sum_{l=1}^{n} \sum_{m=1}^{NGP} e^{-\frac{\Delta t_{s-1}}{\tau_l^E}} \left({}^3\bar{X}_i^{lm}(t_{s-1}) + {}^5\bar{X}_i^{lm}(t_{s-1}) \right) \frac{d\psi_j^{(2)}(x_m)}{dx} \end{aligned} \tag{12.4.74}$$

Similarly, Newton's method results in the following components of the tangent stiffness matrix for the Timoshenko beam theory

$$\begin{gathered} T_{ij}^{11} = \bar{K}_{ij}^{11}, \quad T_{ij}^{12} = T_{ji}^{21} = 2\bar{K}_{ij}^{12}, \quad T_{ij}^{13} = T_{ji}^{31} = 0 \\ T_{ij}^{23} = T_{ji}^{32} = \bar{K}_{ij}^{23}, \quad T_{ij}^{33} = \bar{K}_{ij}^{33} \end{gathered}$$

$$\begin{aligned} T_{ij}^{22} = \bar{K}_{ij}^{22} &+ \int_{x_a}^{x_b} A \left\{ \left(E(0) + \frac{\Delta t_{s-1}}{2} \dot{E}(0) \right) \left[\frac{\partial u}{\partial x} + \left(\frac{\partial w}{\partial x} \right)^2 \right] \right. \\ &\left. + \frac{\Delta t_{s-1}}{2} \dot{E}(\Delta t_{s-1}) \left[\frac{\partial u(x, t_{s-1})}{\partial x} + \frac{1}{2} \left(\frac{\partial w(x, t_{s-1})}{\partial x} \right)^2 \right] \right\} \frac{d\psi_i^{(2)}}{dx} \frac{d\psi_j^{(2)}}{dx} dx \\ &+ \sum_{l=1}^{n} \sum_{m=1}^{NGP} e^{-\frac{\Delta t_{s-1}}{\tau_l^E}} \left({}^3\bar{X}_i^{lm}(t_{s-1}) + {}^4\bar{X}_i^{lm}(t_{s-1}) \right) \frac{d\psi_j^{(2)}(x_m)}{dx} \end{aligned} \tag{12.4.75}$$

12.4.6 Numerical Results

The finite element formulations and procedures developed above are applied to solve quasi-static nonlinear beam deflection problems. For each problem considered, solutions using the EBT and TBT beam theories are compared. The nonlinear beam finite element equations are solved iteratively using the Newton procedure as outlined in the Appendix 2. The solution at a given time step is considered converged once the Euclidean norm of the relative error between two consecutive solutions is less than a pre-selected tolerance. A tolerance of $\varepsilon = 10^{-6}$ is used for all numerical simulations in this study.

It has been noted that the Euler–Bernoulli and Timoshenko beam theories constructed from low-order polynomials suffer from the locking phenomena (see Sections 5.2.7 and 5.3.4; also see [2, 3]). Full integration of the element matrices for the EBT and TBT theories leads to elements that are overly stiff. For the EBT element, full integration leads to membrane locking due to inconsistencies in the interpolation orders of u and w. The TBT elements suffer from membrane locking as well as shear locking in the thin-beam limit. To overcome these shortcomings, one-point Gauss quadrature is used in the evaluation of all nonlinear terms for the EBT finite elements. To eliminate shear and membrane locking from the TBT formulation, elements with high-order Lagrangian interpolation functions are employed. In particular, we introduce the following full integration TBT elements: TBTLN, TBTQD, TBTCB, and TBTQI; which have 2, 3, 4, and 6 nodes (corresponding to linear, quadratic, cubic, and quintic), respectively. Interpolation functions of equal order (i.e. $p_1 = p_2 = p_3$) are utilized for each TBT element.

12.4.6.1 Material properties

For the present analysis we utilize a viscoelastic material model based on the experimental findings of Lai and Bakker [325] for a glassy amorphous polymer material (PMMA). The Prony series parameters for the viscoelastic relaxation modulus given in Table 12.4.1 were calculated from the published compliance parameters [325]. For the Timoshenko beam theory it is also necessary to specify the viscoelastic shear modulus. Although the finite element formulation places no restriction on the relationship between $E\,(t)$ and $G\,(t)$, for the present analysis we adopt the approach taken by Chen [304] and assume that the shear and relaxation moduli are related by

$$G\,(t) = \frac{E\,(t)}{2\,(1+\nu)} \tag{12.4.76}$$

where $\nu = 0.40$ is Poisson's ratio of the material, which is assumed to be independent of time [326].

12.4.6.2 Quasi-static deformation of a beam under uniform load

Here we consider a viscoelastic beam of length $L = 100$ in and cross section 1 in $\times$ 1 in, with material properties given in Table 12.4.1. At $t = 0$ the beam is subjected to a time invariant uniform vertical distributed load $q = 0.25$ lb_f/in.

Table 12.4.1: Viscoelastic material properties.

E_0	205.7818 ksi		
E_1	43.1773 ksi	τ_1^E	9.1955×10^{-1} s
E_2	9.2291 ksi	τ_2^E	9.8120×10^{0} s
E_3	22.9546 ksi	τ_3^E	9.5268×10^{1} s
E_4	26.2647 ksi	τ_4^E	9.4318×10^{2} s
E_5	34.6298 ksi	τ_5^E	9.2066×10^{3} s
E_6	40.3221 ksi	τ_6^E	8.9974×10^{4} s
E_7	47.5275 ksi	τ_7^E	8.6852×10^{5} s
E_8	46.8108 ksi	τ_8^E	8.5143×10^{6} s
E_9	58.6945 ksi	τ_9^E	7.7396×10^{7} s

The computational domain is constructed by taking advantage of the symmetry about $x = L/2$. For the EBT case, ten reduced integration finite elements (11 nodes) are utilized. For the TBT, we consider ten TBTLN elements (11 nodes), four TBTQD elements (9 nodes), three TBTCB elements (10 nodes), and two TBTQI elements (11 nodes). The following three sets of boundary conditions are considered in the analysis:

1. Hinged at both ends (hinged–hinged)

$$w(0,t) = u(L/2,t) = \frac{\partial w}{\partial x}(L/2,t) = 0 \tag{12.4.77}$$

2. Pinned at both ends (pinned–pinned)

$$u(0,t) = w(0,t) = u(L/2,t) = \frac{\partial w}{\partial x}(L/2,t) = 0 \tag{12.4.78}$$

3. Clamped at both ends (clamped–clamped)

$$u(0,t) = w(0,t) = \frac{\partial w}{\partial x}(0,t) = u(L/2,t) = \frac{\partial w}{\partial x}(L/2,t) = 0 \tag{12.4.79}$$

The three cases above are chosen to demonstrate that the EBT and high-order TBT (TBTCB and TBTQI) finite elements do not suffer from the membrane or shear locking phenomena. In addition, each case provides a demonstration of the geometrically nonlinear capabilities of the finite element models that cannot be captured by the uncoupled linear formulation.

The load at $t = 0$ is applied incrementally to ensure convergence of the solution. Five load steps are utilized with a maximum of 20 iterations for each load step. At the first load step, the initial guess vector for the solution is chosen to be the zero vector. This yields the linear solution. At each subsequent iteration within the first load step, the solution vector from the previous iteration is used as the new guess vector. At each new load step, the converged solution from the previous load step is used as the initial guess vector. At each time step following $t = 0$, the finite element equations are solved iteratively using the Newton procedure without the employment of load steps.

Table 12.4.2: Quasi-static analytical and finite element (TBTQI) results for the maximum vertical deflection, w_{max}, of a hinged–hinged viscoelastic beam under uniform distributed load, q.

	Maximum vertical deflection, w_{max}					
Time, t	Exact	$\Delta t = 0.5$	$\Delta t = 1.0$	$\Delta t = 2.0$	$\Delta t = 5.0$	$\Delta t = 10.0$
0	7.2980	7.2980	7.2980	7.2980	7.2980	7.2980
200	8.5429	8.5628	8.6217	8.8492	10.2278	14.7260
400	8.6827	8.7032	8.7641	8.9993	10.4291	15.1493
600	8.7680	8.7891	8.8510	9.0910	10.5524	15.4107
800	8.8364	8.8578	8.9207	9.1645	10.6513	15.6214
1,000	8.8945	8.9160	8.9799	9.2270	10.7356	15.8021
1,200	8.9448	8.9665	9.0311	9.2810	10.8087	15.9597
1,400	8.9886	9.0105	9.0758	9.3282	10.8726	16.0982
1,600	9.0271	9.0492	9.1150	9.3697	10.9288	16.2210
1,800	9.0612	9.0835	9.1498	9.4064	10.9787	16.3306

For the hinged–hinged beam (case 1), the vertical deflection coincides with the exact solution as per the Timoshenko beam theory, which is given by (see Flügge [191] and Reddy [1])

$$w_{max}(t) = \frac{5q_0L^4}{384I}\left[1 + 1.6\,\frac{1+\nu}{K_s}\left(\frac{h}{L}\right)^2\right] D(t) \tag{12.4.80}$$

where $D(t)$ is the creep compliance, which, for the present study, is taken from Lai and Bakker [325]. The solution according to the Euler–Bernoulli theory is obtained by omitting the second term inside the brackets (or by setting $K_s = 0.0$). Table 12.4.2 contains a comparison of the exact Timoshenko beam solution with numerical results obtained using 2 TBTQI beam elements. As is evident from Table 12.4.2, the error in the solution propagates with an increase in time. It is also interesting to note that for the current problem the error incurred by the time step approximation tends to over-predict beam deflections. It is evident that a rather small time step is necessary to ensure convergence.

Table 12.4.3 contains selected numerical results for the quasi-static beam deflection for cases 1 through 3 using the EBT and TBT finite elements. A constant time step $\Delta t = 1.0$ s has been employed with a total simulation time of 1,800 s. Graphical results for EBT, TBTQD, and TBTQI elements are also provided in Fig. 12.4.1. At $t = 0$, the results coincide with the instantaneous elastic solution where the Young's modulus is given as $E = 535.4$ ksi. The

Table 12.4.3: Quasi-static finite element results for the maximum vertical deflection, w_{max}, of a viscoelastic beam under uniform distributed load, q, with three different sets of boundary conditions and $\Delta t = 1.0$.

Time, t	EBT	TBTLN	TBTQD	TBTCB	TBTQI
Hinged–hinged					
0	7.2961	0.8629	7.0098	7.2939	7.2980
200	8.6194	1.0194	8.1966	8.6151	8.6217
400	8.7617	1.0363	8.3221	8.7571	8.7641
600	8.8486	1.0465	8.3986	8.8439	8.8510
800	8.9183	1.0548	8.4598	8.9134	8.9207
1,000	8.9775	1.0618	8.5118	8.9725	8.9799
1,200	9.0287	1.0678	8.5567	9.0236	9.0311
1,400	9.0733	1.0731	8.5958	9.0681	9.0758
1,600	9.1126	1.0778	8.6301	9.1073	9.1150
1,800	9.1474	1.0819	8.6605	9.1420	9.1498
Pinned–pinned					
0	1.2481	0.7258	1.2452	1.2453	1.2452
200	1.3278	0.8210	1.3244	1.3243	1.3242
400	1.3358	0.8307	1.3324	1.3323	1.3322
600	1.3407	0.8366	1.3372	1.3371	1.3370
800	1.3446	0.8413	1.3411	1.3410	1.3409
1,000	1.3478	0.8452	1.3443	1.3442	1.3441
1,200	1.3507	0.8486	1.3471	1.3470	1.3469
1,400	1.3531	0.8516	1.3496	1.3495	1.3494
1,600	1.3553	0.8542	1.3517	1.3516	1.3515
1,800	1.3572	0.8565	1.3536	1.3535	1.3534
Clamped–clamped					
0	0.9110	0.1727	0.8832	0.9102	0.9109
200	1.0000	0.2038	0.9707	0.9988	0.9997
400	1.0089	0.2071	0.9795	1.0077	1.0086
600	1.0144	0.2092	0.9848	1.0130	1.0140
800	1.0187	0.2108	0.9891	1.0173	1.0183
1,000	1.0223	0.2122	0.9927	1.0210	1.0220
1,200	1.0255	0.2134	0.9957	1.0241	1.0251
1,400	1.0282	0.2144	0.9984	1.0268	1.0278
1,600	1.0306	0.2154	1.0008	1.0292	1.0302
1,800	1.0327	0.2162	1.0029	1.0313	1.0323

hinged–hinged beam configuration exhibits greater transverse deflection than the pinned–pinned and clamped–clamped cases. For the hinged–hinged case, the transverse deflection does not lead to significant axial strain, since the hinged ends of the beam are able to translate freely in the x-direction. The pinned–pinned and clamped–clamped beams on the other hand are constrained from axial motion at $x = 0$ and $x = L/2$. As a result, axial strain develops that offers resistance to transverse deformation of the beam.

There is a very good agreement between the numerical results of each formulation with the exception of the TBTLN element which, as expected, suffers

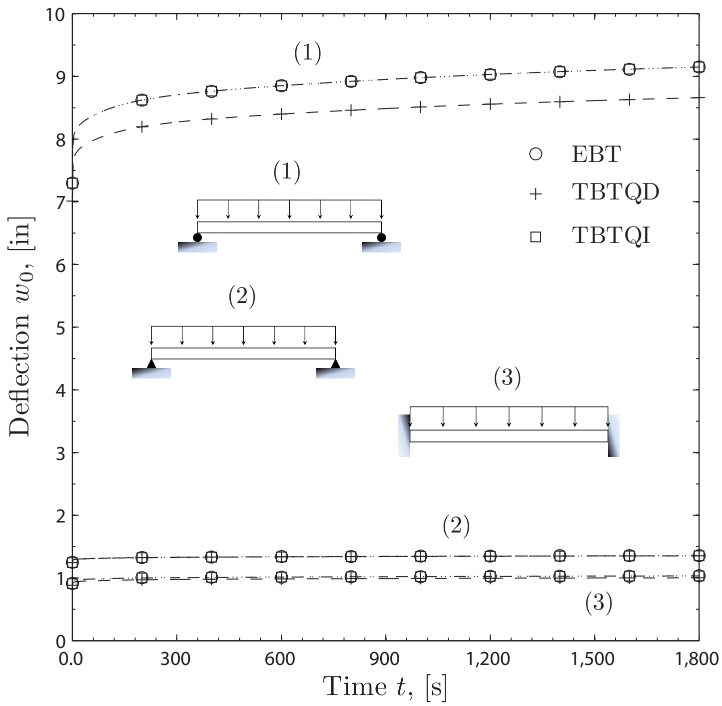

Fig. 12.4.1: Maximum vertical deflection, w_{max}, of a viscoelastic beam under uniform distributed load, q, with three different sets of boundary conditions.

excessively from shear locking. It has been discussed in Chapter 5 that locking can be avoided for this element by employing selective reduced integration. Results for the EBT, TBTCB, and TBTQI are in excellent agreement as the effects of shear deformation are small. Mesh refinement studies of the TBTQI element demonstrate that the presented results for this element are fully converged. In fact, the numerical results presented in Table 12.4.3 for the TBTQI element can be obtained with only one element. The computational cost involved is in fact less with one TBTQI element than any of the other elements, as they require more total nodes for convergence.

An important characteristic of the viscoelastic constitutive model employed here is that the beam should eventually return to its original configuration upon the removal of the loads are. To demonstrate that the finite element models capture this effect, we consider the clamped–clamped beam subject to the following quasi-static transverse load:

$$q(t) = q_0 \Big\{ H(t) - \frac{1}{\tau(\beta - \alpha)} \left[(t - \alpha\tau) H(t - \alpha\tau) - (t - \beta\tau) H(t - \beta\tau) \right] \Big\} \tag{12.4.81}$$

where $q_0 = 0.25$ lb$_\text{f}$/in, $\tau = 1,800$ s, and $H(t)$ is the Heaviside function. The parameters $0 \leq \alpha \leq \beta \leq 1$ are constants. Equation (12.4.81) represents a load function that is constant in $0 < t < \alpha\tau$ and then linearly decreases to zero from $t = \alpha\tau$ to $t = \beta\tau$. For $t > \beta\tau$, the load is maintained at zero. In Fig. 12.4.2 we present numerical results for various values of α and β, where we have employed

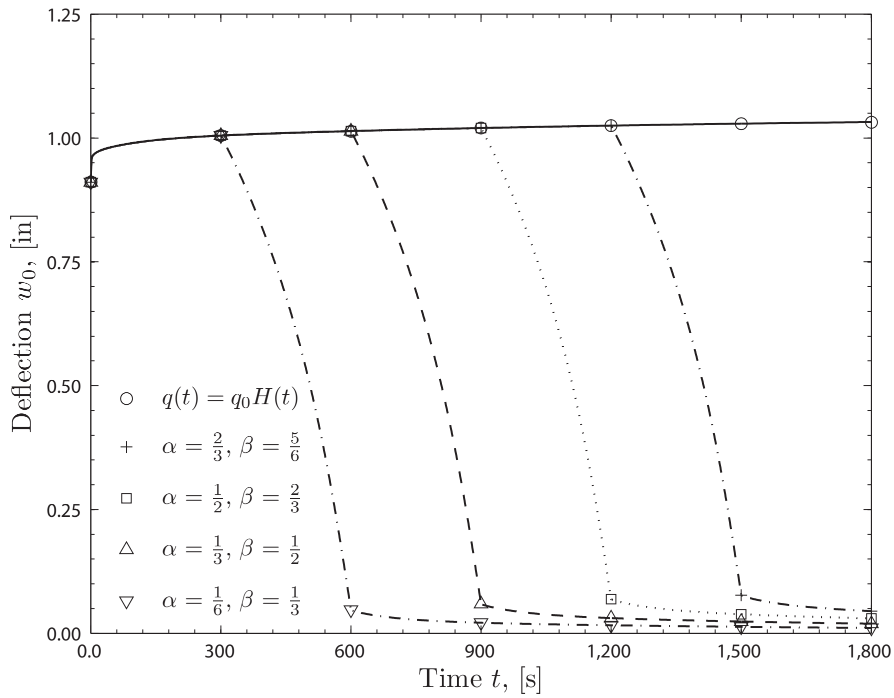

Fig. 12.4.2: Maximum vertical deflection, w_{max}, of a clamped–clamped viscoelastic beam subjected to time-dependent transverse loading $q(t)$.

a constant time step of $\Delta t = 1.0$ s with two TBTQI elements. It is evident that the beam recovers its original configuration as t tends to infinity once the applied load is removed.

We also consider the effect that shear strain has on the transverse deflection of viscoelastic beams. To this end we modify the original thin beam problems by letting $L = 10$ in, $q = 25$ lb$_\text{f}$/in, and $\Delta t = 1.0$ s. All other parameters are kept the same as in the previous examples. In Table 12.4.4 we present numerical results for the transverse deflection of pinned–pinned and clamped–clamped beams using EBT, TBTQD, and TBTQI elements. In all cases we note that the EBT elements under-predict the maximum beam deflections which is as expected.

Table 12.4.4: Effect of shear strain on the maximum quasi-static vertical deflection, w_{max}, of a viscoelastic beam under uniform distributed load, q.

	Maximum vertical deflection, w_{max}					
	Pinned–pinned			Clamped–clamped		
Time t	EBT	TBTQD	TBTQI	EBT	TBTQD	TBTQI
0	0.07184	0.07360	0.07367	0.01459	0.01647	0.01655
200	0.08437	0.08641	0.08649	0.01724	0.01946	0.01955
400	0.08571	0.08777	0.08785	0.01752	0.01978	0.01987
600	0.08652	0.08860	0.08869	0.01769	0.01998	0.02007
800	0.08717	0.08927	0.08935	0.01783	0.02013	0.02023
1,000	0.08773	0.08983	0.08992	0.01795	0.02027	0.02036
1,200	0.08821	0.09032	0.09041	0.01805	0.02038	0.02048
1,400	0.08862	0.09075	0.09083	0.01814	0.02048	0.02058
1,600	0.08899	0.09112	0.09121	0.01822	0.02057	0.02067
1,800	0.08931	0.09145	0.09154	0.01829	0.02065	0.02075

12.5 Summary

In this chapter, finite element models of materially nonlinear elastic and plastic models of one-dimensional problems are presented, and efficient and accurate locking-free linear viscoelastic beam finite elements that are capable of undergoing large transverse displacements, moderate rotations, and small strains are presented. The viscoelastic beam finite element models were developed using the Euler–Bernoulli and Timoshenko beam theories. The discrete form of the finite element equations of viscoelastic beams are constructed using a recurrence relation such that history data need only be stored from the previous time step. Numerical examples are presented to demonstrate the capabilities of the developed numerical models.

Extension of the current formulations to Reddy third-order beam theory can be found in the works of Payette and Reddy [320]. Extensions to plates and shells are of great interest and awaiting attention. In addition, it may also prove useful to extend the current formulation such that more pronounced geometric nonlinearities can be captured (i.e. full geometric nonlinearity). Finally, extension to the case where both material and geometric nonlinearities are accounted for in the formulation is yet to be carried out.

Problems

12.1 Extend the discussion of Section 12.3 to the case of finite strain.

12.2 Extend the discussion of Section 12.3 to Euler–Bernoulli beams made of elastic material with constitutive relation $\sigma_{xx} = E\varepsilon_{xx}$, where E is given by

$$E = E_0 + E_1\left[\frac{du}{dx} + \frac{1}{2}\left(\frac{dw}{dx}\right)^2\right] \tag{1}$$

where E_0 and E_1 are functions of x only. Assume linear strain-displacement relations:

$$\varepsilon_{xx} = \varepsilon_{xx}^{(0)} + z\varepsilon_{xx}^{(1)}; \quad \varepsilon_{xx}^{(0)} = \frac{du}{dx}, \quad \varepsilon_{xx}^{(1)} = -\frac{d^2w}{dx^2} \tag{2}$$

12.3 Extend Problem 12.2 to the case with the von Kármán nonlinear strain

$$\varepsilon_{xx} = \frac{du}{dx} + \frac{1}{2}\left(\frac{dw}{dx}\right)^2 - z\frac{d^2w}{dx^2}$$

12.4 Extend the discussion of Section 12.3 to Timoshenko beams made of a material whose constitutive relation is the same as that given in Problem 12.2 (with a constant Poisson's ratio). Use the following strain-displacement relations of the Timoshenko beam theory:

$$\varepsilon_{xx} = \frac{du}{dx} + \frac{1}{2}\left(\frac{dw}{dx}\right)^2 + z\frac{d\phi_x}{dx}, \quad \gamma_{xz} = \phi_x + \frac{dw}{dx}$$

12.5 (*Reddy beam theory*) Develop the weak-forms associated with the nonlinear quasi-static and fully transient analysis of initially straight viscoelastic beams using the following kinematic assumptions of the third-order Reddy beam theory [3, 55, 56]:

$$\begin{aligned} u_1(x,y,z,t) &= u(x,t) + z\phi_x(x,t) - z^3c_1\left(\phi_x(x,t) + \frac{\partial w}{\partial x}\right) \\ u_2(x,y,z,t) &= 0 \\ u_3(x,y,z,t) &= w(x,t) \end{aligned} \tag{1}$$

where the $x = X$ (material) coordinate is taken along the beam length, the $z = Z$ coordinate along the thickness direction of the beam, u is the axial displacement of a point on the mid-plane $(x, 0, 0)$ of the beam and w represents the transverse deflection of the mid-plane. When the deformation is small the parameter $\phi_x(x,t)$ may be interpreted as the rotation of the transverse normal. The constant c_1 is equal to $c_1 = 4/(3h^2)$, where h is the height of the beam and b is the beam width. The displacement field of the Reddy beam theory suggests that a straight line perpendicular to the undeformed mid-plane becomes a cubic curve following deformation, as can be seen in Fig. P12.5.

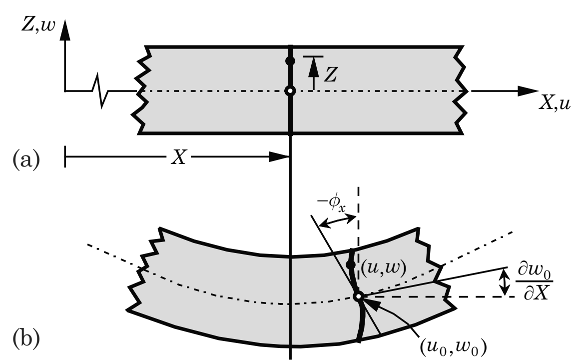

Fig. P12.5: (a) Undeformed configuration and (b) deformed configuration.

12.6 (continuation of *viscoelastic Reddy beam finite element*) Develop the semidiscrete viscoelastic finite element model of the Reddy third-order beam theory.

12.7 (continuation of *viscoelastic Reddy beam finite element*) Develop the fully discrete viscoelastic finite element model of the Reddy third-order beam theory (i.e. give the linearized equations in the Newton's method).

References

NOTE: The reference numbers used here are a continuation of the numbers from the main (printed) book.

285. R. Hill, *The Mathematical Theory of Plasticity*, Oxford University Press, Oxford, U.K. (1950).
286. W. Johnson and P. B. Mellor, *Engineering Plasticity*, John Wiley, New York (1983).
287. A. S. Khan and S. Huang, *Continuum Theory of Plasticity,* John Wiley, New York (1995).
288. A. R. Srinivasa and S. M. Sivakumar, *Inelasticity of Materials: An Engineering Approach and Practical Guide,* World Scientific, Singapore (2009).
289. D. R. J. Owen and E. Hinton, *Finite Elements in Plasticity: Theory and Practice*, Pineridge Press, Swansea, UK (1980).
290. K. Krabbenhft, *Basic Computational Plasticity,* Lecture Notes, Department of Civil Engineering, Technical University of Denmark (2002).
291. W. Flügge, *Viscoelasticity*, 2nd ed., Springer, Berlin, Heidelberg (1975).
292. R. M. Christensen, *Theory of Viscoelasticity,* 2nd ed., Academic Press, New York (1982).
293. N. Phan-Thien, *Understanding Viscoelasticity, Basics of Rheology,* Springer, Berlin (2008)
294. S. Roy and J. N. Reddy, *Computational Modelling of Polymer Composites, A Study of Creep and Environmental Effects,* CRC Press, Boca Raton, Florida (2013).
295. A. S. Wineman and K. R. Rajagopal, *Mechanical Response of Polymers: An Introduction,* Cambridge University Press, New York (2000).
296. W. N. Findley, J. S. Lai, and K. Onaran, *Creep and Relaxation of Nonlinear Viscoelastic Materials,* North–Holland, New York (1976).
297. R. L. Taylor, K. S. Pister, and G. L. Goudreau, "Thermomechanical analysis of viscoelastic solids," *International Journal for Numerical Methods in Engineering*, **2**, 45–59 (1970).
298. J. T. Oden and W. H. Armstrong, "Analysis of nonlinear dynamic coupled thermoviscoelasticity problems by the finite element method," *Computers and Structures,* **1**, 603–621 (1971).
299. G. A. Holzapfel and G. Reiter, "Fully coupled thermomechanical behaviour of viscoelastic solids treated with finite elements," *International Journal of Engineering Science*, **33**(7), 1037–1058 (1995).
300. S. Yi, S. F. Ling, M. Ying, H. H. Hilton, and J. R. Vinson, "Finite element formulation for anisotropic coupled piezoelectro-hygro-thermo-viscoelasto-dynamic problems," *International Journal for Numerical Methods in Engineering*, **45**, 1531–1546 (1999).
301. S. Hartmann, "Computation in finite-strain viscoelasticity: finite elements based on the interpretation as differential-algebraic equations," *Computer Methods in Applied Mechanics and Engineering*, **191**, 1439–1470 (2002).

302. F. Cortés and M. J. Elejabarrieta, "Finite element formulations for transient dynamic analysis in structural systems with viscoelastic treatments containing fractional derivative models," *International Journal for Numerical Methods in Engineering*, **69**, 2173–2195 (2007).
303. J. J. Rencis, S. Saigal, and K.-Y. Jong, "Dynamic viscoelastic beam model for finite element method," *Journal of Aerospace Engineering,* **3**(1), 19–29 (1990).
304. T.-M. Chen, "The hybrid Laplace transform/finite element method applied to the quasi-static and dynamic analysis of viscoelastic Timoshenko beams," *International Journal for Numerical Methods in Engineering*, **38**(1), 509–522 (1995).
305. Y. Aköz and F. Kadioğlu, "The mixed finite element method for the quasi-static and dynamic analysis of viscoelastic Timoshenko beams," *International Journal for Numerical Methods in Engineering*, **44**, 1909–1932 (1999).
306. B. Temel, F. F. Calim, and N. Tütüncü, "Quasi-static and dynamic response of viscoelastic helical rods," *Journal of Sound and Vibration*, **271**, 921–935 (2004).
307. Z. Zheng-you, L. Gen-guo, and C. Chang-jun, "Quasi-static and dynamical analysis for viscoelastic Timoshenko beam with fractional derivative constitutive relation," *Applied Mathematics and Mechanics,* **23**(1), 1–12 (2002).
308. Q. Chen and Y. W. Chan, "Integral finite element method for dynamical analysis of elastic-viscoelastic composite structures," *Computers and Structures,* **74**, 51–64 (2000).
309. M. A. Trindade, A. Benjeddou, and R. Ohayon, "Finite element modeling of hybrid active-passive vibration damping of multilayer piezoelectric sandwich beams-part I: Formulation," *International Journal for Numerical Methods in Engineering,* **51**, 835–854 (2001).
310. A. Pálfalvi, "A comparison of finite element formulations for dynamics of viscoelastic beams," *Finite Elements in Analysis and Design*, **44**, 814–818 (2008).
311. D. J. McTavish and P. C. Hughes, "Finite element modeling of linear viscoelastic structures," *The Role of Damping in Vibration and Noise Control,* **5**, 9–17 (1987).
312. D. J. McTavish and P. C. Hughes, "Modeling of linear viscoelastic space structures," *Journal of Vibration and Acoustics,* **115**, 103–110 (1993).
313. V. Balamurugan and S. Narayanan, "Finite element formulation and active vibration control study on beams using smart constrained layer damping (SCLD) treatment," *Journal of Sound and Vibration*, **249**(2), 227–250 (2000).
314. V. Balamurugan and S. Narayanan, "Active-passive hybrid damping in beams with enhanced smart constrained layer treatment," *Engineering Structures,* **24**, 355–363 (2002).
315. A. R. Johnson, A. Tessler, and M. Dambach, "Dynamics of thick viscoelastic beams," *Journal of Engineering Materials and Technology*, **119**, 273–278 (1997).
316. E. M. Austin and D. J. Inman, "Modeling of sandwich structures," *SPIE*, **3327**, 316–327 (1998).
317. A. C. Galucio, J. F. Deü, and R. Ohayon, "Finite element formulation of viscoelastic sandwich beams using fractional derivative operators," *Computational Mechanics*, **33**, 282–291 (2004).
318. G. Ranzi and A. Zona, "A steel-concrete composite beam model with partial interaction including the shear deformability of the steel component," *Engineering Structures*, **29**, 3026–3041 (2007).
319. G. S. Payette and J. N. Reddy, "Nonlinear quasi-static finite element formulations for viscoelastic Euler–Bernoulli and Timoshenko beams," *International Journal for Numerical Methods in Biomedical Engineering,* **26**(12), 1736–1755 (2010).
320. G. S. Payette and J. N. Reddy, "A nonlinear finite element framework for viscoelastic beams based on the high-order Reddy beam theory," *Journal of Engineering Materials and Technology,* **135** (1), 011005-1 to 011005-11 (2013).

321. V. P. Vallala, G. S. Payette, and J. N. Reddy, "Spectral/hp finite element formulation for viscoelastic beams based on an higher-order beam theory, *International Journal of Applied Mechanics,* **4**(1), 1–28 (2012).
322. V. P. Vallala, A. Ruimi, and J. N. Reddy, "Nonlinear viscoelastic analysis of orthotropic beams using a general third-order theory," *Composite Structures,* **94**, 3759–3768 (2012).
323. J. N. Reddy, "On locking-free shear deformable beam finite elements," *Computer Methods in Applied Mechanics and Engineering,* **149**, 113–132 (1997).
324. J. C. Simo and T. J. R. Hughes, *Computational Inelasticity,* Springer–Verlag, Berlin (1998).
325. J. Lai and A. Bakker, "3-D Schapery representation for non-linear viscoelasticity and finite element implementation," *Computational Mechanics,* **18**, 182–191 (1996).
326. D. W. Van Krevelen, *Properties of Polymers*, 3rd ed., Elsevier, Amsterdam, The Netherlands (1990).